J|A|C|S
ARTICLES
Published on Web 01/18/2002

Solubilized, Spaced Polyalanines: A Context-Free System for Determining Amino Acid α-Helix Propensities

Justin S. Miller,† Robert J. Kennedy, and Daniel S. Kemp*
Contribution from the Department of Chemistry, Room 18-582, Massachusetts Institute of Technology, Cambridge, Massachusetts 02139

Received July 16, 2001

Abstract: The logical design principles behind a system of properly water-solubilized, spaced polyalanines are presented. Peptides conforming to these design principles are shown to be unaggregated, and their helical properties as measured by the circular dichroism (CD) residue ellipticity at 222 nm, $[\theta]_{222}$, are shown to be dependent upon the lengths of their alanine regions. It is further demonstrated that CD contributions of the alanine cores are independent of the CD contributions attributable to other features of the peptides. The CD response of these polyalanines to variations in temperature and salt or denaturant concentration is described. CD data for a series of peptides with Ala_n cores varying in length from 12 to 45 residues are presented that allow calculation of the helical propensity, w_{Ala}, in a purely alanine context. Mathematical modeling of these unprecedented data reveals the insufficiency of currently accepted literature helicity modeling parameters. A modification to the standard Lifson−Roig algorithm is introduced based on hydrogen-bonding cooperativity.

Introduction

Alanine is the simplest of the helix-favoring amino acids, and polyalanines are the obvious hosts for exploring helix-stabilizing and destabilizing effects of guest amino acids that bear more complex side chains. By correlating such effects, one hopes to assign both intrinsic amino acid helical propensities (*w* values) and correction terms. These include helix stability changes that arise from context-dependent interactions between particular neighboring residues and site-dependent effects that reflect differences of helical structure or local charge within core or ends of a helical conformation. A helical propensity is an equilibrium constant that reflects the tendency of a pre-existing helical conformation to add a particular type of new amino acid residue. If the helical conformation contains residues neighboring the site of addition that interact strongly with the new residue, the resulting propensity includes context-dependent effects, but if these are minimal as expected for a helical polyalanine, the resulting experimental propensity can be defined as intrinsic. Assignment of the intrinsic helical propensity of alanine is a necessary preliminary to the use of polyalanines as hosts for separation and analysis of propensities and correction terms for other amino acids. This assignment has proved to be difficult.

Peptides composed solely of alanine residues are useless as hosts since they aggregate and exhibit low water solubility, but it has long been recognized that nonpolar hydrophobic peptides such as polyalanines can be rendered water soluble if N- and C-capped by strongly hydrophilic or charged peptide sequences composed of residues such as lysine or glutamate.[1] An alternative approach to solubilization was reported in 1989 by Marqusee, Robbins, and Baldwin,[2] who characterized aqueous solutions of highly helical unaggregated peptides containing sequences $(A_4X)_x$, $x = 3-5$, X = K (or E) in which solubilizing residues are spaced within alanine sequences. Subsequently the helical properties of alanine residues within these solubilized peptides were taken to approximate those within a simple polyalanine, and the peptide helicities were interpreted to imply that alanine has an exceptionally large helical propensity. Numerical values in the range of $1.6 \leq w \leq 1.9$ have been assigned.[3] Later it was argued that the observed helicities of medium-sized polyalanines that are capped by positively charged, solubilizing residues are also consistent with this range of *w* assignment.[4,5]

Other interpretations are possible. Charged caps[6] or interior residues may significantly bias stabilities of the helical conformations of short alanine peptides. Definitive experimental evidence on this critical point has been lacking, but the Scheraga group has proposed plausible helix-stabilizing mechanisms for lysine residues in alanine-rich contexts and has drawn attention to the inconsistency of a high alanine helical propensity with

† Present Address: Sloan−Kettering Institute for Cancer Research, Laboratory for Bioorganic Chemistry, 1275 York Avenue, Box 106, RRL 1349, New York, NY 10021.

(1) (a) Ingwall, R. T.; Scheraga, H. A.; Lotan, N.; Berger, A.; Katchalski, E. *Biopolymers* **1968**, *6*, 331−368. (b) Gratzer, W. B.; Doty, P. *J. Am. Chem. Soc.* **1963**, *85*, 1193−1197. (c) Rothwarf, D. M.; Davenport, V. G.; Shi, P.-T.; Peng, J.-L.; Scheraga, H. A. *Biopolymers* **1996**, *39*, 531−536.
(2) Marqusee, S.; Robbins, V. H.; Baldwin, R. L. *Proc. Natl. Acad. Sci. U.S.A.* **1989**, *86*, 5286−5290.
(3) (a) Chakrabartty, A.; Kortemme, T.; Baldwin, R. L. *Protein Sci.* **1994**, *3*, 843−852. (b) Park, S.-H.; Shalongo, W.; Stellwagen, E. *Biochemistry* **1993**, *32*, 7048−7053.
(4) Rohl, C. A.; Fiori, W.; Baldwin, R. L. *Proc. Natl. Acad. Sci. U.S.A.* **1999**, *96*, 3682−3687.
(5) Spek, E. J.; Olson, C. A.; Shi, Z.; Kallenbach, N. R. *J. Am. Chem. Soc.* **1999**, *121*, 5571−5572.
(6) (a) Harper, E. T.; Rose, G. D. *Biochemistry* **1993**, *32*, 7605−7609. (b) Schneider, J. P.; DeGrado, W. F. *J. Am. Chem. Soc.* **1998**, *120*, 2764−2767. (c) Esposito, G.; Dhanapal, B.; Dumy, P.; Varma, V.; Mutter, M.; Bodenhausen, G. *Biopolymers* **1997**, *41*, 27−35. (d) Aurora, R.; Rose, G. D. *Protein Sci.* **1998**, *7*, 21−38.

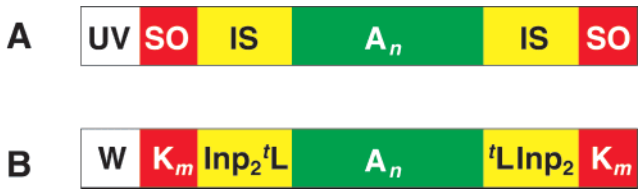

Figure 1. Schematic depicting properly solubilized, spaced polyalanines. The upper diagram represents the desired features of such peptides, with a reporting UV chromophore (white) for concentration determination, two solubilizing SO regions (red) separated from the alanine A_n core (green) by a pair of isolating spacers IS (yellow) that do not allow interactions between the core and capping regions. The lower diagram illustrates the structures developed here for each of these features: the UV chromophore is a tryptophan (W) residue, the solubilizers are short oligolysines, and the novel IS regions each consist of two isonipecotic acid (Inp) residues and a *tert*-leucine (^{t}L) residue.

results from their earlier experiments.[7,8] The conclusions of the Scheraga group were in accord with our own findings from NMR studies of helicity of Ala peptides that are N-capped with a novel reporting conformational template Ac-Hel.[9] The alanine helical propensities reported by the Scheraga and Kemp groups lie in the range of $1.03 \leq w \leq 1.15$, much smaller than those assigned from study of the charge-solubilized alanine-rich peptides. Doubt has recently been cast on the validity of our NMR analysis of the Ac-Hel-A_n-NH_2 series,[4,5] which owing to insolubility cannot be extended beyond six residues. Analyses of hosts consisting of helical peptide bundles and small helical proteins have usually ranked alanine as the strongest helix former, but these differ significantly in the degree to which the helical propensity of alanine exceeds that of the other helix-stabilizing amino acids.[10]

Assignment of the intrinsic alanine helical propensity thus has been mired in controversy, reflecting disagreements concerning appropriate hosts, measurement techniques, and the size of site and context effects of neighboring charge-bearing amino acids. At issue are two fundamental questions. Can one construct an accurate algorithm for predicting peptide helicity from helical propensities that are not intrinsic? Does the range of reported w_{Ala} values reflect methodological errors, or should it be attributed to differences in the local features of the peptide or protein contexts in which these parameters have been measured? These questions can only be addressed and resolved by the helicity standard provided by a solubilized, unaggregated, helical polyalanine that is demonstrably unperturbed by side chain, charge, or capping-dependent stabilizing or destabilizing factors.

Results and Discussion

We now report water-solubilized helical polyalanines of defined length that allow the first characterization of helicity properties intrinsic to alanine. In a recent communication we introduced the concept of peptide N- and C-caps that both solubilize and isolate a core peptide.[11] The underlying general principle is shown in the schematic of Figure 1, and the accompanying amino acid sequence is the optimized working example that is developed in this report.

This report starts with an analysis that validates both the concept and the sequence of Figure 1. We then characterize the circular dichroism properties of a series of Figure 1 polyalanines Ala_n between 12 and 45 residues in length. Finally we report results of Lifson−Roig analyses that assign intrinsic helical propensities for alanine.

Circular dichroism spectroscopy (CD) is the most widely used tool for quantitating polypeptide helicity.[12] Because of its nearly universal acceptance and its experimental efficiency, we used it in our feasibility studies that led to the sequence of Figure 1. This sequence has been optimized for CD measurements at low millimolar to micromolar concentrations in water. NMR-based helix characterizing techniques may require higher peptide concentrations; we have recently introduced a variant of this sequence that is suitable for this purpose.[13]

CD-optimized isolating N- and C-caps contain three functions, as seen in Figure 1: an ultraviolet reporter for concentration determination, a solubilizing region SO, and a spacing region IS that isolates the core polyalanine of interest from helix-perturbing effects of SO. Helicity is usually quantitated as $[\theta]_{222}$, the residue ellipticity at 222 nm, in part because of the weak or negligible contributions of other peptide conformations at this wavelength. We restricted our choices for IS and SO regions to candidates that are unlikely to form or join helices and thus do not contribute significantly to $[\theta]_{222}$. Proving this point was a major goal of the feasibility phase of this project.

The concentration of a peptide used in a CD measurement must be known accurately in order to characterize $[\theta]$. Concentrations are usually calculated from the observed UV optical density and known molar extinction coefficient ϵ at λ_{max} of a Tyr (Y) or Trp (W) residue, incorporated at or near an end of the peptide sequence. Unless properly spaced from it, either residue can perturb the helical peptide CD spectrum in an unpredictable manner.[14] We selected Trp because of its greater extinction coefficient ϵ at a longer λ_{max}. The larger ϵ allowed accurate concentration measurements on solutions that could be used without dilution for CD studies. As noted in the Appendix, we tested the concentration, site, and medium independence of the Trp ϵ at 280 nm, finding $\epsilon_{280} = 5.56 \times 10^3$ M^{-1} cm^{-1}, in accord with literature values.[15] Partly for maximum convenience in purification following conventional solid-phase peptide synthesis, Trp was usually sited at the peptide N-terminus, isolated from the alanine core by SO and IS regions. As reported in a later section, using test peptides with constant core, SO, and IS regions, calculated values for $[\theta]_{222}$ were shown to be independent of placement of W at N- or C-terminal sites.

Solubilization and suppression of aggregation have previously been reported for triblock copolymers in which an alanine oligopeptide served as the core, flanked by charged polylysine or polyglutamate end regions.[1] In the 1966 study by Gratzer and Doty,[1b] a core polyalanine sequence containing approxi-

(7) Vila, J.; Williams, R. L.; Grant, J. A.; Wójik, J.; Scheraga, H. A. *Proc. Natl. Acad. Sci. U.S.A.* **1992**, *89*, 7821−7825.
(8) Scheraga, H. A. In *Perspectives in Structural Biology*; Vijayan, M., Yathindra, N., Kolaskar, A. S., Eds.; Indian Academy of Sciences: Bangalore, 1999; pp 275−292.
(9) Kemp, D. S.; Allen, T. J.; Oslick, S. L. *J. Am. Chem. Soc.* **1996**, *118*, 4249−4255.
(10) Williams, L.; Kather, K.; Kemp, D. S. *J. Am. Chem. Soc.* **1998**, *120*, 11033−11043.
(11) Miller, J. S.; Kennedy, R. J.; Kemp, D. S. *Biochemistry* **2001**, *40*, 305−309.
(12) (a) Sears, D. W.; Beychok, S. In *Physical Principles and Techniques of Protein Chemistry, Part C*; Leach, S. J., Ed.; Academic Press: New York, 1973; pp 445−593. (b) Woody, R. W. *J. Polym. Sci. Macromol. Rev.* **1977**, *12*, 181−321.
(13) Kennedy, R. J.; Kemp, D. S. *J. Am. Chem. Soc.* **2002**, *124*, 934−944.
(14) Chakrabartty, A.; Kortemme, T.; Padmanabhan, S.; Baldwin, R. L. *Biochemistry* **1993**, *32*, 5560−5565.
(15) Mihalyi, E. *J. Chem. Eng. Data* **1968**, *13*, 179−182.

mately 175 residues was flanked by a pair of poly-DL-glutamate sequences of overall length 325 residues; it was found to be soluble in aqueous phosphate buffer and judged to lack significant aggregation by the methods of that time. Solubilization was not observed for an alanine oligopeptide linked to a single polyglutamate block. A water-soluble triblock polymer reported by the Scheraga group contained a short polyalanine region flanked by polylysines.[1c] We have not explored poly(ethylene glycol) conjugates of peptides as solubilizers, although their practicality has been demonstrated by an extensive literature, and they may prove suitable for generating isolating, capping constructs.[16]

Primarily for experimental convenience, we have selected short N- and C-terminal oligolysine regions for the SO functions as shown in Figure 1. Ease and consistency of high-performance liquid chromatography (HPLC) purification and mass spectroscopy (MS) characterization are greatly facilitated by the large pH window ($0 < pH < 10$) in which the peptide is a polycation. High charge density in the SO regions also influences the form of their CD spectra. Owing to heightened electrostatic repulsion in compact states such as helices, polylysine at a pH below 10 adopts extended, unstructured conformations and is expected to make minimal contributions to $[\theta]_{222}$.[17,18]

The positive charge of these SO regions also posed a design challenge for the IS spacers. Whether one attributes the effect to the presence of an overall helix dipole[19] or to local electrostatic effects of the oriented amides at the ends of helices,[20] an abundant literature demonstrates significant stabilization of helices by a negative charge sited at an N-terminus and by a positive charge at a C-terminus. A functional IS spacer must screen the alanine core from the positively charged SO region.

We briefly considered and then rejected N- and C-terminal SO functions bearing opposing charges. In principle they offer a very elegant test of the efficiency of candidates for the IS region. If charge leakage occurs, owing to charge−helix dipole interactions, one would expect different core helicities for the potentially stabilizing sequence $Glu_mISAla_nISLys_mNH_2$ and its potentially destabilizing permutation isomer $Lys_mISAla_nISGlu_mNH_2$. When two examples of the latter were prepared, they were found to be insoluble in water, while examples of the former, though soluble, showed CD evidence of aggregation as well as visible precipitation at 60 °C.

Development of Effective IS Functions. The IS region is our novel design feature. Ultimately any feasible IS structural candidate must be shown to leave the helicity attributable to the alanine core invariant when small structural changes are made in any of the UV, IS, or SO regions. During the design stages, the planning of experiments was guided by the anticipated interactions between the core and a particular IS candidate. If interactions of the core with SO charges are deemed likely for a particular IS candidate, then it must be screened for these interactions as a first experimental priority. Even if an IS candidate effectively isolates the core and SO regions, it might fail by extending the helix beyond the core boundaries. This would occur if IS amino acid residues at the IS−core junction are capable of assuming helical conformations and forming new helical hydrogen bonds, lengthening the helix to an unpredictable degree. Rigorous helicity analysis requires $[\theta]_{222}$ values, calculated by dividing the experimental molar ellipticity $[\theta]_{222,molar}$ by the maximum length n of the helix. If n is ill-defined owing to possible IS helical extension, $[\theta]_{222}$ cannot be calculated accurately.

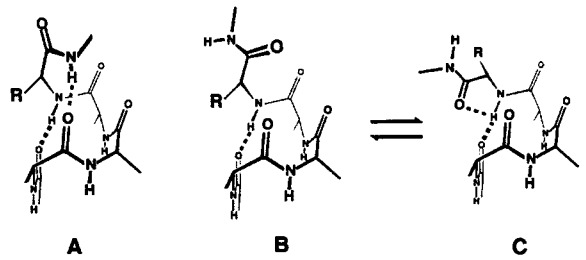

Figure 2. The C-terminal residue (with side chain R) can terminate a helix while providing a final hydrogen bond (B and C) or extend a helix (A). The C-capping H-bond may be normal (B), or it may be perturbed by the neighboring carbonyl moiety (C), depending upon the conformational equilibrium between the structures represented in (B) and (C) (see ref 43).

As seen in Figure 2B and C, a C-cap that terminates a helix must contribute a single helical H-bonding site to it by providing a proximal amide NH. A helix-extending amino acid at a peptide C-terminus, Figure 2A, can form two helical H-bonds if its ϕ and ψ dihedral angles are consistent with helical structure and it bears an additional H-bonding site that provides a new, distal amide NH. An equivalent argument applies to capping or extending residues at a helix N-terminus.

The absence of extension and distal H-bonding would be ensured if the residues at the core boundary of an IS candidate lack the capacity to form new helical hydrogen bonds or if its ϕ or ψ angles are very strongly biased against helices. Since N- and C-capping residues can strongly influence the helicity of a peptide,[6,21] rigorous Lifson−Roig calculations of core helicity thus must include capping parameters that reflect the helicity influence of IS residues at the core boundary.

At early stages of the testing process for a particular IS candidate, before we have proved the absence of helical extension within the IS region, we use $[\theta]_{222,molar}$ rather than $[\theta]_{222}$ to compare relative helicities. We assign residue ellipticities only for peptides bearing IS regions that have been proved to confine the helix to the core region and to insulate it from SO interactions. For these cases maximum helical length n is defined as the length of the polyalanine core.

Short polyglycines have often been incorporated at points within designer protein sequences where elements of defined secondary structure must be isolated or where exceptional chain flexibility is desired. Glycine is usually assigned a small helical propensity, presumably reflecting the structural permissiveness of its backbone. Potential flexibility need not guarantee a high capacity to isolate strongly interacting peptide regions. The large area of (ϕ,ψ) space open to the glycine backbone includes very compact regions that are inaccessible to other amino acid residues and that may permit enthalpically favorable interactions between charged residues and the core. The flexibility of polyglycines is dependent on what is presumed to be an unfavorable tradeoff between the large entropy associated with

(16) Pillai, V. N. R.; Mutter, M. *Acc. Chem. Res.* **1981**, *14*, 122−130.
(17) Woody, R. W. *Advances in Biophysical Chemistry*; JAI Press: Greenwich, CT, 1992; Vol. 2, pp 37−79.
(18) Greenfield, N.; Fasman, G. D. *Biochemistry* **1969**, *8*, 4108−4115.
(19) (a) Hol, W. G. J.; van Duijnen, P. T.; Berendsen, H. J. C. *Nature (London)* **1978**, *273*, 443−445. (b) Hol, W. G. J.; Halie, L. M.; Sander, C. *Nature (London)* **1981**, *294*, 532−534.
(20) Tidor, B. *Proteins: Struct., Funct. Genet.* **1994**, *19*, 310−323.
(21) Doig, A. J.; Baldwin, R. L. *Protein Sci.* **1995**, *4*, 1325−1336.

a random populating of the energetically accessible regions of the Ramachandran diagram and a potentially large opposing enthalpy of stabilization attributable to a few compact polyglycine conformations that permit helix−charge interactions. If the latter are sufficiently stabilizing, flexibility may not be a dependable feature of polyglycines.

Can a polyglycine IS region permit linear extension of the helix? Although Gly is usually assigned a small helical propensity if it is sited in core regions of a helical sequence,[3a,22] isolated reports support the premise that it can extend a helix at its ends.[23] Moreover, it may act as a helix-stabilizing cap.[24] These doubts must be explored in feasibility studies for polyglycine IS regions.

For feasibility studies, we picked test peptides from the general sequence $WK_3G_jA_{12}G_kK_3NH_2$. An alanine core length of 12 was chosen since Lifson−Roig modeling suggests that $[\theta]_{222}$ for a helix in this length range should be maximally responsive to capping stabilization and to the value of the intrinsic alanine helical propensity w.[25] For $w \geq 1.6$, readily detectable CD helicity is predicted even if capping stabilization is absent, but for $w \leq 1.15$ and for a helix that lacks capping stabilization, the observed CD spectrum should lack helical features and should be indistinguishable from that of an unstructured peptide.

If polyglycine spacers do not participate in helix extension and have lengths j, k sufficient to prevent significant interactions between the solubilizers and a 12-residue core, then $[\theta]_{222,\mathrm{molar}}$ should be unchanged if j or k is increased or if the nature of the solubilizer is modified. Polyglycines with $2 \leq j$ or $k \leq 7$ fail to meet either of these tests. The $[\theta]_{222,\mathrm{molar}}$ values continue to increase to a spacer length of 7 glycine residues, at which point aggregation is observed.[26] Moreover, replacement of the solubilizing K_3 elements by other positively charged amino acid residues changes $[\theta]_{222,\mathrm{molar}}$ significantly. (See Table S2 in the Supporting Information.) This failure of the polyglycine candidates is epitomized by the comparison of Figure 3, which shows partially helical CD spectra observed for a permutation pair that contains polyglycine sequences of unequal length. The observed strong dependence of $[\theta]_{222,\mathrm{molar}}$ on the order of the spacing elements is inconsistent with the defining features of an isolating spacer. The similarity of $[\theta]_{222,\mathrm{molar}}$ values that is observed for the pairs of spacing elements G_2, G_2 and G_2, G_4 as well as G_4, G_4 and G_4, G_2 implies a greater helical sensitivity to the N-terminal spacing distance, as noted in the figure legend.

The remaining candidates for isolating spacers employ rigidity to achieve two aims. The rigid spacer must place sufficient distance between the alanine core and the solubilizers to attenuate direct or solvent-mediated interactions between these regions. It must also confine the helical length of the core to the polyalanine region by capping it with amino acid residues that have minimal tendency to join a helix and thus do not extend its length. As the most conformationally restricted of the natural amino acids, proline is an obvious building block

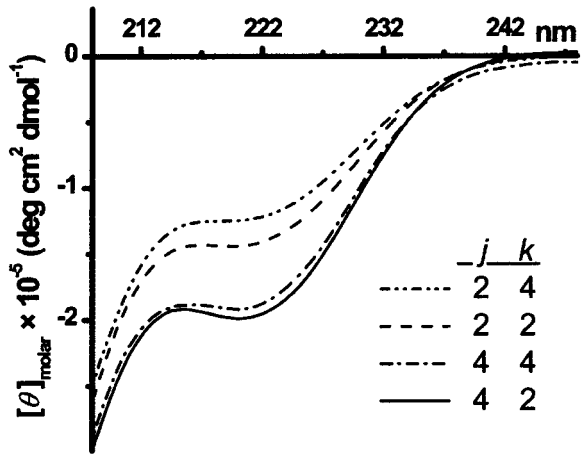

Figure 3. CD spectra in water of peptides $WK_3G_jA_{12}G_kK_3NH_2$ with variable length glycine spacers. CD dependence at 222 nm upon the lengths of the spacers invalidates glycine IS candidates. The plot indicates a stronger dependence on the N-terminal spacing length j than on the C-terminal spacing length k, consistent with the hypothesis that flexible glycine spacers extend to prevent unfavorable charge−core interactions at the N-terminus but collapse to allow a favorable interaction at the C-terminus.

for constructing an isolating spacer. The preferred conformations of polyproline have been well characterized by modeling and X-ray crystallography. Proline residues have also been noted to appear frequently at the N-terminal regions of α-helices in globular proteins.[27]

By virtue of its C-terminating a polypeptide sequence with a backbone tertiary amide, proline must prevent the final residue of a core sequence from contributing a C-terminal helical hydrogen bond. In effect, it shortens the helix by one residue at its C-terminus. The energetic significance of this point is unclear, since the helix C-terminus is unlikely to embody a normal helical hydrogen-bonding geometry.

We have also examined short sequences of unnatural amino acids as isolating spacers. The achiral proline analogue isonipecotic acid (Inp, 4-carboxypiperidine) maximizes both rigidity and linear extension as noted in Figure 4. Unlike P and Inp, the exceptionally hindered acyclic α-amino acid *tert*-leucine (^{t}L, α-*tert*-butylglycine) yields peptides that retain the normal peptide amide backbone structure. Its bulky *tert*-butyl group selectively stabilizes extended conformations in preference to helices.[28] Helical peptides containing single or multiple ^{t}L groups have been studied, and CD analysis shows that ^{t}L is compatible with helical structure but has a very small helical propensity, and when multiple ^{t}L residues are sited in a peptide core it inhibits helical propagation.[29] Figure 4 shows the structure of $^t L_3$ and compares spacing distances for Inp_3, $^t L_3$, and $^t LInp_2$.

As documented in a review by Woody,[17] the CD spectra of unstructured polypeptides are characterized by an intensely negative ellipticity minimum in the neighborhood of 190 nm, which decreases in intensity and approaches zero at ca. 210 nm. The region of 210−230 nm may show no significant structure but often exhibits a weak positive ellipticity maximum at around 215−220 nm. Figure 5 shows CD spectra of peptides of sequence $WK_3ISA_{12}ISK_3NH_2$, where IS is composed of P_3,

(22) Wójik, J.; Altmann, K.-H.; Scheraga, H. A. *Biopolymers* **1990**, *30*, 121−134.
(23) (a) Dyson, H. J.; Rance, M.; Houghten, R. A.; Wright, P. E.; Lerner, R. A. *J. Mol. Biol.* **1988**, *201*, 201−217. (b) Zerkowski, J.; Powers, E. T.; Kemp, D. S. *J. Am. Chem. Soc.* **1997**, *119*, 1153−1154.
(24) Aurora, R.; Srinivasan, R.; Rose, G. D. *Science* **1994**, *264*, 1126−1130.
(25) See Figure 15, which demonstrates that peptides of length 12 are sensitive to the value of w.
(26) $WK_3G_7A_{12}G_7K_3$ exhibits properties consistent with aggregation in 0.1 M NaCl solution.
(27) Levitt, M. *Biochemistry* **1978**, *17*, 4277−4285.
(28) Ramnarayan, K.; Chan, M. F.; Balaji, V. N.; Profeta, Jr., S.; Rao, S. N. *Int. J. Pept. Protein Res.* **1995**, *45*, 366−376.
(29) (a) Lyu, P. C.; Sherman, J. C.; Chen, A.; Kallenbach, N. R. *Proc. Natl. Acad. Sci. U.S.A.* **1991**, *88*, 5317−5320. (b) Hermans, J.; Anderson, A. G.; Yun, R. H. *Biochemistry* **1992**, *31*, 5646−5653.

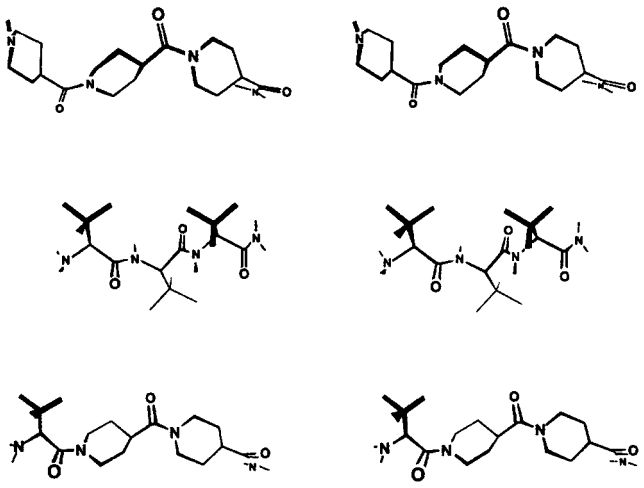

Figure 4. Stereodiagrams of three rigid spacers. Achiral Inp_3 (top) demonstrates maximal linear extension, spanning an Nα to C(=O) distance of 13.4 Å, but like Pro_3 cannot provide a C-terminal H-bond. The extended conformation of $^tL_3$ (middle) is highly favored, but ^tL can be compatible with helical structure and spans only 9.2 Å. The hybrid C-terminal spacer $^tLInp_2$ (bottom) embodies the extension of Inp, with a total spacing distance of 13.1 Å, while completing the final C-terminal helical H-bond by virtue of its extended ^tL residue proximal to the helical core. Conformations and distances were calculated using Quanta 98 from Molecular Simulations, Inc.

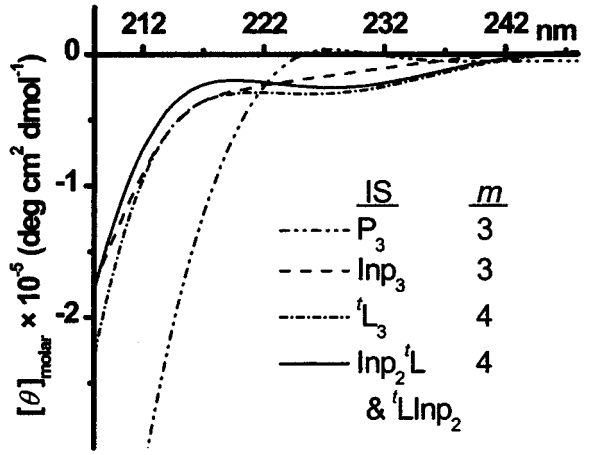

Figure 5. CD spectra in water of peptides $WK_mISA_{12}ISK_mNH_2$ with variable rigid spacers. The near-identity of $[\theta]_{222,molar}$ for these peptides is a strong indication that rigid spacers are effective IS candidates.

Inp_3, and $^tL_3$. These spectra are all characteristic of unstructured peptides and lack helical features. As expected, the short-wavelength ellipticities are most intense for IS = P_3.

Also shown in Figure 5 is the CD spectrum of the peptide $WK_4Inp_2{}^tLA_{12}{}^tLInp_2K_4NH_2$, in which hybrid spacers are used that N- and C-cap the alanine core with ^tL residues. We have not rigorously defined the minimum spacer length required to suppress solubilizer−core interactions, although we believe it to lie in the size range of one to three amino acid residues. Thus, CD spectra for the sequence $WK_3Inp_gA_{12}Inp_gK_3NH_2$ with g = 1, 2, or 3, yield indistinguishable, small values for $[\theta]_{222,molar}$. Single spacing residues were compared for the peptides $WK_3ISA_{12}ISK_3NH_2$, where IS = P, Inp, or ^tL. Although spectra characteristic of unordered peptides were again observed, it is perhaps suggestive that for IS = ^tL, $[\theta]_{222,\ molar}$ has a small negative value that marginally exceeds the limit of values attributable to the capping residues. It would be expected that ^tL would be the least efficient of the three types of rigid spacing residues. The observation that $[\theta]_{222,molar}$ for all four members of this series are identical within experimental error and close to zero is a necessary first step toward validating the class of rigid spacers as IS candidates. As noted below, the variations in $[\theta]$ that are seen in these spectra for $\lambda < 220$ nm can be attributed to contributions from the capping regions.

Diagnostics in Helical Peptides. A more definitive validation requires study of an alanine core sequence that exhibits significant CD ellipticity. A 19-residue alanine sequence $WK_4ISA_{19}ISK_4NH_2$ fulfills this role. A satisfactory IS candidate must show an invariant $[\theta]_{222,molar}$ if spacers are varied within the rigidity manifold, if the site of the W chromophore within the capping regions is varied, and if the solubilizers are varied. The A_{19} peptides exhibit CD spectra characteristic of moderately structured helices with $[\theta]_{222,molar}$ values of -5.16×10^5 for IS = Inp_3, -5.06×10^5 for IS = P_3, and -5.16×10^5 for the IS N, C pair $Inp_2{}^tL$ and $^tLInp_2$; these values are identical within measurement limits. The general sequence $WK_mInp_2{}^tLA_n{}^tLInp_2K_mNH_2$ was used in all subsequent studies; henceforth n refers to the residue length of the alanine core and m denotes the length of the lysine solubilizers. This sequence contains IS functions that flank the alanine region with ^tL residues capable of forming normal backbone secondary amides.

We next explored the sensitivity of $[\theta]_{222,molar}$ to the site of placement of the UV reporter W, using the fixed sequence $K_mInp_2{}^tLA_n{}^tLInp_2K_m$, n = 19, m = 4. Three peptides were prepared: two contained single W residues positioned either at the N- or the C-terminus, and the the third contained W residues positioned at both sites. The respective $[\theta]_{222,molar}$ values were -5.16×10^5, -5.06×10^5, and -5.16×10^5, showing their insensitivity to the site of the UV reporter function.

CD Independence of the Core and Capping Regions. The remaining test involves changes in the solubilizers. For the above comparisons we have reported $[\theta]_{222,molar}$ data rather than the full CD spectra, which are expected to be dissimilar at short wavelength owing to the significant contributions of the spacing and solubilizing elements. A more rigorous test of the efficacy of the rigid spacing pair $Inp_2{}^tL$ and $^tLInp_2$ involves correction of CD spectra of a series of capped peptides $WK_mInp_2{}^tLA_n{}^tLInp_2K_mNH_2$ with helical cores by subtracting the contributions of the capping regions as estimated from model peptides. If the spacers are properly operative, the CD spectra of helical capped peptides at all wavelengths should be, to an excellent approximation, a simple sum of contributions of ellipticities from core and capping regions, and the difference spectra should be invariant.

To define the CD contributions of the caps, we selected peptide sequences in which the alanine core length n was chosen to be long enough to maintain the CD characteristics of the junction between each rigid spacer and the alanine region, but short enough that the contribution of alanine to the overall $[\theta]_{222,molar}$ is effectively insignificant. Figure 6A shows CD spectra of the series where n = 4 and the length of the solubilizing regions m ranges from 2 to 7. These CD spectra embody the features expected for peptides with unordered conformations.[17] Significantly, $[\theta]_{molar}$ values measured at short wavelength increase nearly linearly with the number of lysine residues, implying that the lysine-containing portions of the solubilizing regions define the major part of the CD chromophores

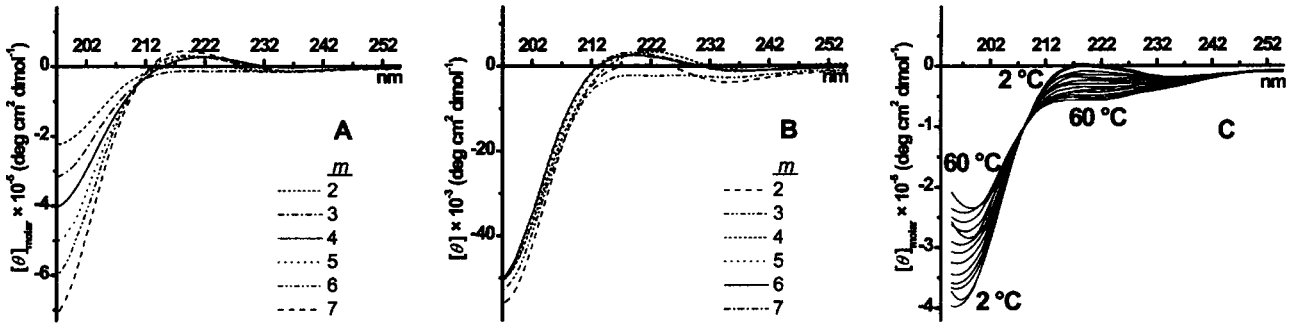

Figure 6. CD spectra of $WK_mInp_2{}^tLA_4{}^tLInp_2K_mNH_2$ in water of solubilized, spaced peptides with core alanine regions four residues in length. When molar ellipticities obtained at 2 °C (A) are divided by the total length $2m$ of the lysine solubilizing regions, nearly identical CD curves (B) are obtained. These peptides demonstrate little dependence of $[\theta]_{222}$ upon solubilizer length m; the representative case for which $m = 4$ also exhibits only small $[\theta]_{222,molar}$ over a range of temperatures (C) from 2 °C and at 5 °C intervals between 5 and 60 °C.

for these molecules; the data in Figure 6B displaying the spectra from Figure 6A on a per lysine residue basis illustrate this point. It is clear from these data that, as expected, the capping regions do not contribute significantly to $[\theta]_{222,molar}$. The data in Figure 6C for the representative peptide with $m = 4$ also indicate that the capping regions do not contribute significantly to $[\theta]_{222,molar}$ over a wide temperature range from 2 to 60 °C.

Figure 7A shows the CD spectra for $n = 19$ with $m = 3$, 4, and 7; when these are corrected for the contributions of their capping regions by subtracting the corresponding spectra from Figure 6A and divided by the number of Ala residues, the three difference spectra of Figure 7B are obtained. These spectra are identical within the error of measurement at all wavelengths and show the CD signature expected for a stabilized helical conformation: strong positive ellipticity at wavelengths below 200 nm with a strong negative minimum at 208 nm and also at 222 nm. The near identity of these difference spectra validates the hypothesis that the CD spectra of Figure 7A can be accurately approximated as sums of independent contributions of core and caps and that the spacing elements $Inp_2{}^tL$ and ${}^tLInp_2$ are effective IS candidates. In these cases there is no significant interaction between the solubilizers and the core. We can now define the helix length for these difference spectra as 19 residues, the length of the alanine core, and report ellipticities at 222 nm on a per residue basis.

Freedom from Aggregation. The remaining point to be demonstrated is freedom from aggregation at CD concentrations in water. Simple intuition and the classical experiments on helical regions of triblock polymers suggest that as the length n of the hydrophobic core region of $WK_mInp_2{}^tLA_n{}^tLInp_2K_mNH_2$ is increased beyond some limit, continued control of solubility and aggregation requires an increase in the length m of the solubilizing sequence. As with spacer length we have not explored this point rigorously, but using the preliminary criterion of aggregation as evidenced by the appearance of structured, nonhelical CD spectra, we conclude that for $m = 4$, the upper limit for core length n is approximately 28 residues. Increasing the value of m to 5 allowed study of conjugates with lengths n between 29 and 36 residues, and a further increase to $m = 6$ permitted study at low salt and at CD concentrations of core peptides with $n = 44$ and 45. Although it appears likely that longer core peptides can be studied, particularly in light of literature reports on the behavior of triblock polymers, $n = 45$ is the longest alanine conjugate that we have prepared and characterized. Helical CD spectra were observed for peptides A_{19}, A_{28}, and A_{45} at low micromolar concentrations, either in pure water or in the presence of 0.1 M NaCl, although in the latter solvent, the A_{45} peptide showed an unusual lack of temperature dependence.

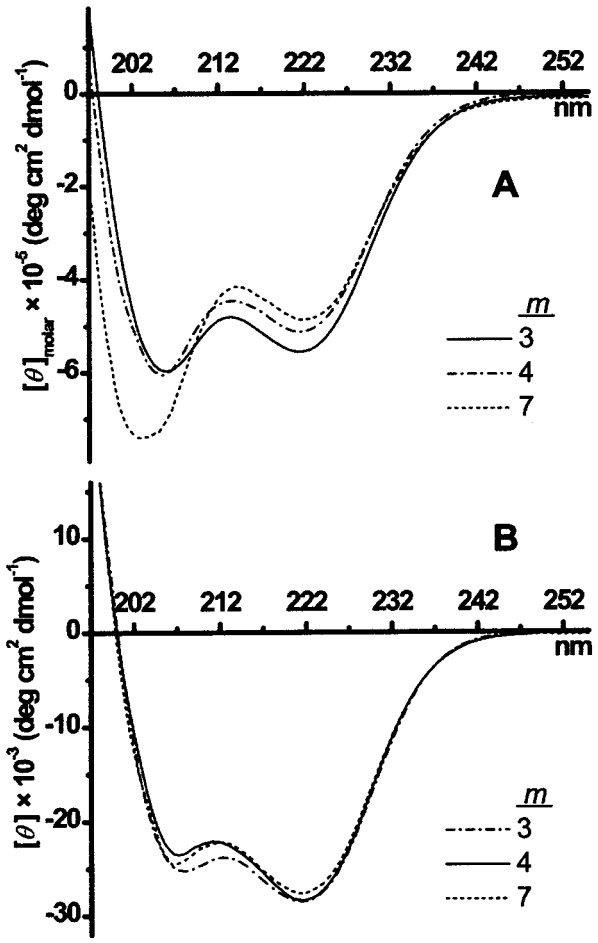

Figure 7. CD spectra for peptides with 19-residue alanine cores and variable-length lysine solubilizers in water at 2 °C. The CD spectra (A) show only a small dependence of $[\theta]_{222,molar}$ upon solubilizer length m. Corrected for CD capping contributions (B), the spectra can be expressed on a per residue basis, to yield $[\theta]$, and are coincident within error. They provide the first CD characterization of a context-free polyalanine helix of medium length. From modeling reported in a later section, the fractional helicity of this peptide is approximately 50%.

Equilibrium analytical ultracentrifugation (AUC) tests were applied to the three peptides with $n = 19$, 28, and 45 to establish rigorously that aggregation is minimal under CD conditions. The results are summarized in Figure 8.

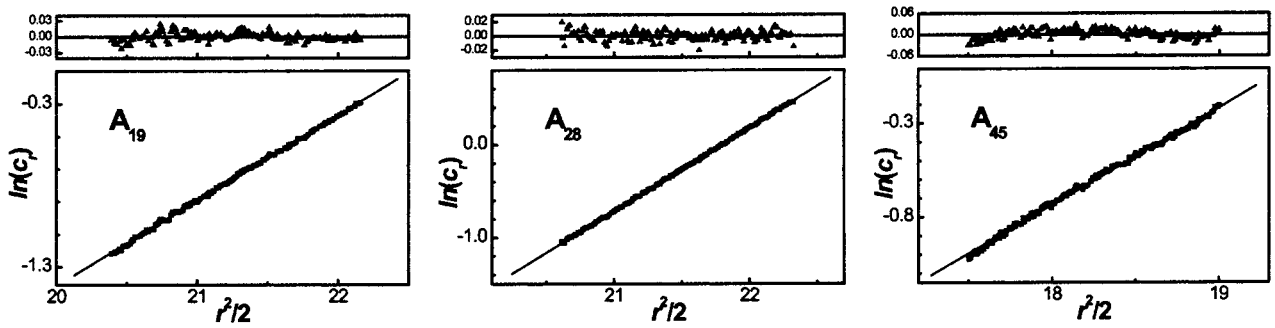

Figure 8. AUC results for solubilized, spaced polyalanines. The data for the peptides with core lengths 19 residues (left) and 28 residues (middle) and solubilizer length $m = 4$ were gathered in 0.1 M NaCl solution; straight-line fits yield molecular weights within 7% of those found by mass spectroscopy. Although the peptide with a 45-residue core was aggregated in aqueous salt, the data for A_{45} in pure water (right) with $m = 6$ are easily fitted to a straight line; the peptide is therefore unaggregated in pure water.

When equilibrium is reached in an ultracentrifugation experiment, at each point in the cell the flux of diffusing molecules must equal the opposing flux of sedimenting molecules.[30] For a single molecular weight species under these conditions, the buoyant mass M_b obeys eq 1, where r is the distance to the

$$\ln c_r = M_b \frac{\omega^2}{2RT} r^2 \qquad (1)$$

rotation center, c_r is the solute concentration at radial distance r from the rotation axis, ω is the rotor speed, R is the gas constant, and T is temperature. A plot of ln c_r is strictly linear in r^2 for such a species; all three graphs in Figure 8 meet this linearity criterion, consistent with the absence of detectable aggregation for the $n = 19$, $n = 28$, and $n = 45$ conjugates under the conditions of the experiment.

The buoyant mass M_b, easily calculable from the slope of the plot of ln c_r vs r^2, is related to the actual molecular mass M by eq 2, where $\bar{v}$ is the partial spatial volume occupied by the

$$M_b = M(1 - \bar{v}\rho) \qquad (2)$$

molecule in solution and ρ is the solvent density. For ultracentrifugation experiments on typical globular proteins, accurate estimates of the partial specific volume of the molecule $\bar{v}$ can be obtained as sums of empirical values for the component amino acids, and provided sufficient salt is added to completely suppress solute−solute electrostatic interactions, values within ±3% for the molecular mass can be calculated from eq 2. Our solubilized polyalanine conjugates are manifolds of conformations of widely varying length, no conformation is compact, and each bears a substantial positive charge. They are therefore relatively poor candidates for this calculation. Nonetheless, as noted in the legend accompanying Figure 8, calculations of the molecular weights for the peptides with $n = 19$ and 28 in 0.1 M NaCl from the slopes of the plot of ln c_r vs r^2 using standard values of $\bar{v}$ and ρ agree with the masses established by mass spectroscopy within 7%.

Equilibrium ultracentrifugation of A_{45} confirmed the presence of aggregate in 0.1 M NaCl but gave the linear correlation in pure water that is shown in Figure 8. This molecule bears an overall positive charge of 13, and in the absence of sufficient salt to effectively screen electrostatic solute−solute interactions, the molecular weight calculated from eq 2 is expected to be significantly lower than the true value. In fact, the calculated molecular weight in pure water is roughly half the mass spectrometric value, and this result was confirmed by carrying out ultracentrifugation in D_2O, which has a significantly larger solvent density ρ. Consistent with their CD spectra, in water each of the three species studied thus shows behavior in the ultracentrifuge indicative of an unaggregated species.

Effects of Temperature, Salt, and Denaturant on CD Properties of Solubilized, Spaced Polyalanines. We have synthesized, purified, characterized by mass spectrometry, and subjected to CD measurement in water at 2, 25, and 60 °C, 19 capped polyalanine peptides with the general structure $WK_mInp_2{}^tLA_n{}^tLInp_2K_mNH_2$. These comprise 14 examples with $m = 4$ and n from 12 to 28 residues; three examples with $m = 5$ and $n = 29$, 35, 36; and two examples with $m = 6$ and $n = 44$, 45. After subtraction of the corresponding CD capping contributions at the appropriate temperatures and lengths m of the lysine solubilizers, their CD ellipticities are reported as $[\theta]$ calculated using the number of alanines in their cores. Henceforth in this text, these homoalanine conjugates are referred to simply as A_n. Figure 9 depicts corrected temperature-dependent CD spectra in water for A_{16}, A_{19}, and A_{28} at 2 °C and at intervals of 5 °C between 5 and 60 °C.

The spectra of Figure 9 show several notable features. A substantial temperature variation in $[\theta]_{222}$ is noted for all of these homoalanine oligomers, but convergence to a high-temperature limit is not seen, implying that helix melting is incomplete at 60 °C. The general form of the temperature-dependent spectra for A_{16} is consistent with a helical peptide manifold that is dominated by nonhelical conformations, but these also must contribute at lower abundance to the A_{19} and A_{28} spectra. The significant temperature changes seen in $[\theta]_{222}$ near 0 °C show that convergence to a limiting low-temperature spectrum has not occurred. The spectra for A_{16}, A_{19}, and A_{28} in pure water thus correspond to frayed helices with fractional helicities significantly less than 1.0, as predicted from Zimm−Bragg or Lifson−Roig models.[31] The presence of an isoellipsoidal region at ca. 203 nm with $[\theta]_{203}$ in the range of $(-15 \text{ to } -17) \times 10^{-3}$ deg cm^2 dmol^{-1} suggests that in this region CD spectra are approximated by linear combinations of unordered and helical spectra.[32] However, a simple two-state model gives a poor fit to $[\theta]$ values at longer wavelengths. Such a model requires linearity of a parametric plot of $[\theta]_{222}$ vs $[\theta]_{208}$, but for A_{19} and

(30) Tanford, C. *Physical Chemistry of Macromolecules*; John Wiley and Sons: New York, 1961; pp 180−272.

(31) (a) Zimm, B. H.; Bragg, J. *J. Phys. Chem.* **1959**, *31*, 526−535. (b) Lifson, S.; Roig, A. *J. Phys. Chem.* **1961**, *34*, 1963−1974.

(32) Holtzer, M. E.; Holtzer, A. *Biopolymers* **1992**, *32*, 1675−1677.

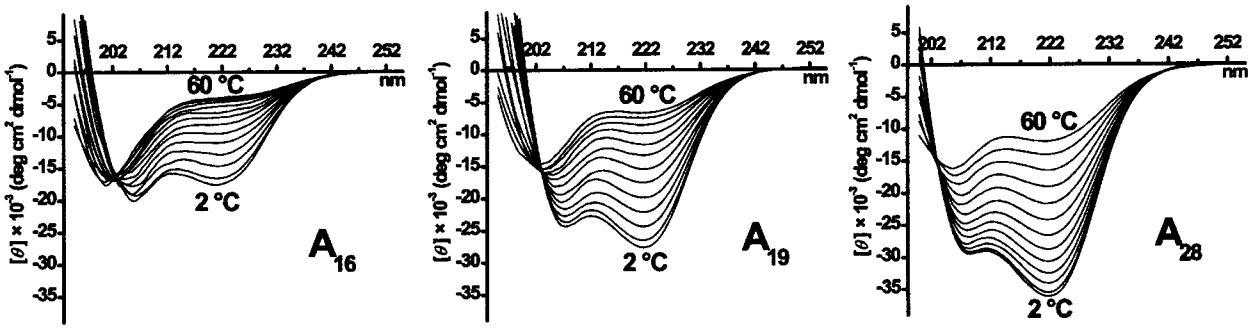

Figure 9. Temperature-dependent CD spectra of A_{16}, A_{19}, and A_{28} in water at 2 °C and at intervals of 5 °C between 5 and 60 °C. A_{16} displays the least and A_{28} the most helical character at all temperatures. All three show significant melting at higher temperatures. Their temperature-dependent CD properties are consistent with those of peptides of similar length and composition.

A_{28} data at low temperatures, such plots show strong upward curvature. The significance of this finding lies outside the scope of this report but will be analyzed subsequently.

Tied to this curvature are the unusually large ellipticity ratios $[\theta]_{222}/[\theta]_{208} = R2$ that are evident at low temperature for the A_{19} and A_{28} data. This ratio was proposed by Gierasch and coworkers as a measure of helicity,[33] with the expectation that a classic helical CD spectrum should have an $R2$ value close to 1.0. Other alanine-rich helical peptides have previously been reported to show larger $R2$ values in water at low temperatures,[34] and we have demonstrated this effect to be general for alanine-rich, lysine-containing peptides that are N-capped by the helix initiator Ac-Hel.[35] The data of Figure 9 demonstrate that $R2$ values in the range of 1.1−1.3 must be an intrinsic property of highly helical, hydrated, unaggregated alanine-rich peptides. The significance of this finding will be discussed subsequently.

Many literature reports address salt and denaturant effects for polypeptide helices. In this study we sought to establish consistency between our results and earlier reports and to define practical working conditions for future applications of the spaced, solubilized polyalanines. The effects of varying concentrations of NaCl or the denaturant guanidine hydrochloride (GuHCl) on the CD spectra of the 19-residue oligomer were measured at 2, 25, and 60 °C and are shown respectively in Figures 10 and 11. No detectable dependence of $[\theta]_{222}$ on NaCl concentration was observed in the dilute range up to 0.1 M, as seen in Figure 10. Our data lie within experimental error of the modest change in this low salt region that has been reported for other uncharged helical peptides,[36] and we conclude that for polyalanines, CD measurements made in water alone should be indistinguishable from those made at low salt. Depicted in Figure 11 is the dependence of $[\theta]_{222}$ on the concentration of the denaturant guanidine hydrochloride (GuHCl) at 2, 25, and 60 °C. The nearly linear dependences observed for A_{19} are unremarkable and resemble those reported for other simple helical peptides in water.[2]

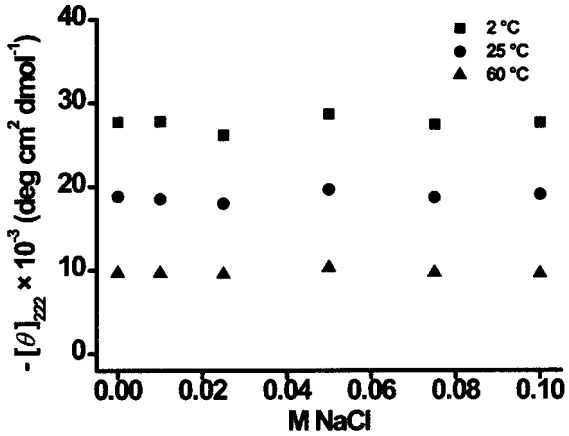

Figure 10. Dependence of $[\theta]_{222}$ for $WK_4Inp_2{}^tLA_{19}{}^tLInp_2K_4$ upon the concentration of sodium chloride up to 0.1 M at 2, 25, and 60 °C (uncorrected values). Although not a perfect diagnostic, the lack of a salt dependence in this concentration range is consistent with the absence of charge effects upon the helix.

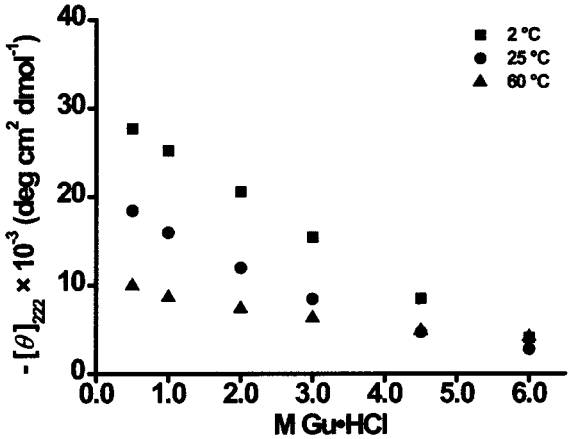

Figure 11. Dependence of $[\theta]_{222}$ for $WK_4Inp_2{}^tLA_{19}{}^tLInp_2K_4$ upon the concentration of the denaturant guanidine hydrochloride (GuHCl) up to 6.0 M at 2, 25, and 60 °C (uncorrected values). This behavior of A_{19} is expected for a helix manifold destabilized by the presence of denaturant.

Length- and Temperature-Dependent CD Properties of Solubilized, Spaced Polyalanines, and Correlation with the Lifson−Roig Model. Figure 12 plots $-[\theta]_{222}$ as a function of the length of A_n ranging from 12 to 45 residues at temperatures of 2, 25, and 60 °C in water, and Figure 13 plots $-[\theta]_{222}$ as a function of temperature for the specific lengths $n = 16$, 19, and 28 residues. These plots allow semiquantitative correlation with the predictions of the Lifson−Roig helicity model, with assignment of upper and lower bounds for w_{Ala}.

(33) Bruch, M. D.; Dhingra, M. M.; Gierasch, L. M. *Proteins: Struct., Funct. Genet.* **1991**, *10*, 130−139.
(34) (a) Merutka, G.; Stellwagen, E. *Biochemistry* **1991**, *30*, 1591−1594. (b) Merutka, G.; Shalongo, W.; Stellwagen, E. *Biochemistry* **1991**, *30*, 4245−4248. (c) Scholtz, J. M.; Marqusee, S.; Baldwin, R. L.; York, E. J.; Stewart, J. M.; Santoro, M.; Bolen, D. W. *Proc. Natl. Acad. Sci. U.S.A.* **1991**, *88*, 2854−2858.
(35) Wallimann, P.; Kennedy, R. J.; Kemp, D. S. *Angew. Chem., Int. Ed.* **1999**, *38*, 1290−1292.
(36) (a) Merutka, G.; Lipton, W.; Shalongo, W.; Park, S.-H.; Stellwagen, E. *Biochemistry* **1990**, *29*, 7511−7515. (b) Shalongo, W.; Dugad, L.; Stellwagen, E. *J. Am. Chem. Soc.* **1994**, *116*, 8288−8293. (c) Scholtz, J. M.; York, E. J.; Stewart, J. M.; Baldwin, R. L. *J. Am. Chem. Soc.* **1991**, *113*, 5102−5104.

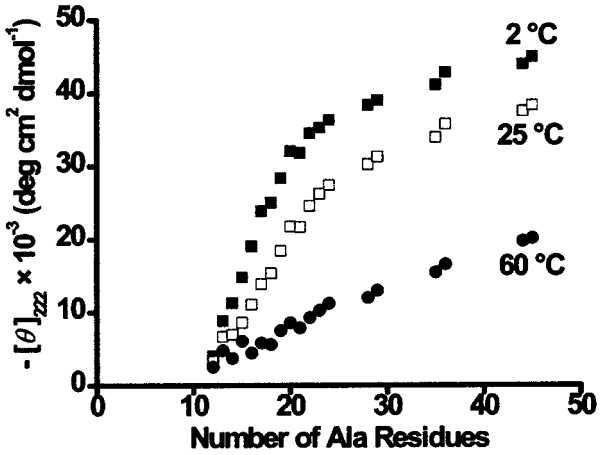

Figure 12. Ellipticity at 222 nm plotted vs core length *n* for polyalanines 12−45 residues long at 2, 25, and 60 °C. This is the first such comprehensive dataset for context-free polyalanines of known length. These data can be used to test the assumptions of homopeptide helicity models.

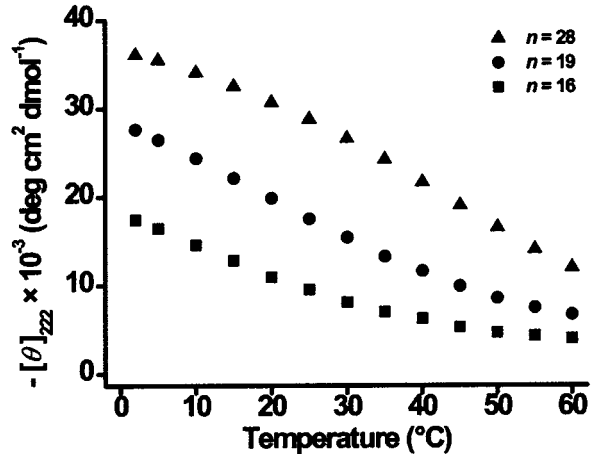

Figure 13. Temperature dependence of $[\theta]_{222}$ for A_{16}, A_{19}, and A_{28} in water at 2 °C and at intervals of 5 °C between 5 and 60 °C. All three peptides melt gradually over a large temperature range, consistent with conformational manifolds containing a variety of helical lengths.

The L−R algorithm allows calculation of fractional helicity (f_H) of a spaced, solubilized polyalanine as a function of three parameters, the maximum length *n* of its helical region, the helical propensity w_{Ala} which decreases with temperature, and the helical initiation constant υ, usually taken to be temperature independent, and has been assigned[37] a frequently cited value of 0.048. According to current usage, at constant *n*, f_H is taken as proportional to $[\theta]_{222}$. For a peptide of length *n* the qualitative features of a plot of $-[\theta]_{222}$ vs temperature (e.g., Figure 13) closely resemble those of a plot of f_H vs *w*, which results directly from application of the L−R algorithm. Similarly, a plot of $-[\theta]_{222}$ vs *n* at a particular temperature (e.g., Figure 12) resembles a plot of f_H vs *n* at fixed *w*. As detailed in the next section, this qualitative introduction to the problem of assigning w_{Ala} is appropriate because the function that relates f_H to $-[\theta]_{222}$ is currently controversial.

How does the L−R algorithm generate f_H from *w*, υ, and *n*? The algorithm treats an isolated helical peptide in solution as a conformational manifold composed of nonhelical, partially helical, and completely helical states. The relative abundance of each state is governed by a mass action product of an unfavorable initiation parameter, defined as υ^2, and a series of marginally favorable helical propensities *w*. The overall f_H is a sum of contributions of state f_H values for conformations containing partial helices of length $k \leq n$. Each can be written as $(k/n)\chi_k$, where χ_k is the mole fraction of conformations with helical regions of length *k*. Summing this expression from $k = 3$ to *n* then gives f_H, as shown in eq 3.

$$f_H = \sum_n^k \chi_k \qquad (3)$$

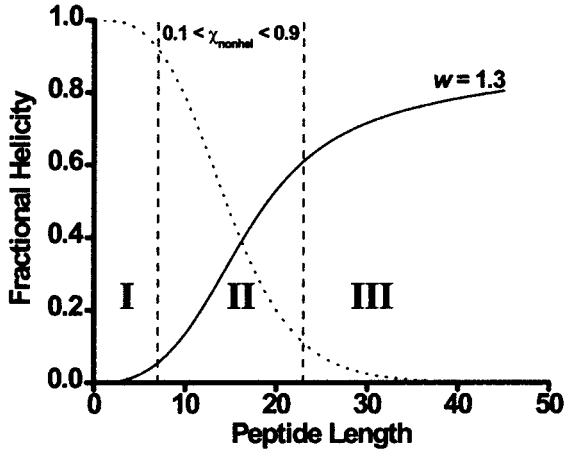

Figure 14. Fractional helicity plotted vs homopeptide length *n* for $\upsilon = 0.048$ and $w = 1.3$. Shown by the dotted line is a plot of $\chi_{nonhelical}$ vs length *n*. In length region I most of the molecules contain no helical segments. Peptides in the intermediate length region II rapidly become more helical with increasing length because longer helices are more stable. Most of the peptides in region III contain helices, but the ever-increasing number of conformations that are not fully helical competes with the stability gained by the longest helices with increasing length.

The length dependence of f_H is informative. Figure 14, calculated for $\upsilon = 0.048$ and $w = 1.3$, is typical. Included in this graph is a plot of the length dependence of the corresponding mole fraction of nonhelical conformations, $\chi_{nonhelical}$, which can be used to identify three length regions within the figure, each with a characteristic signature at the molecular level.

In the first region, defined by $\chi_{nonhelical} > 0.9$, the conformations of most molecules lack helices. Helicity is experimentally undetectable within this region. The width of region I decreases with increasing *w* since the exponential w^k determines the weight of each helical conformation, and f_H becomes significant only when the cumulative weight of w^k terms overcomes the unfavorable initiation penalty, υ^2. In region II, the average $\chi_{nonhelical}$ is less than 0.5 and drops dramatically with increasing length *n*. The slope of the plot in this region is maximal because the majority of molecules now contain helical conformations that become more stable and more numerous as each additional residue is added to the length. Throughout region III, $\chi_{nonhelical}$ is negligible, and the slope of the length plot decreases substantially but does not become zero. For accessible lengths *n* and plausible values of *w*, the fractional helicity in region III remains less than 1.0. This effect occurs because the mole fraction of the completely helical conformation in region III remains relatively small, and the conformational population continues to be dominated by partially helical molecules. The slope is small because as *n* increases, e.g. from 50 to 51 residues, even though the weight of the completely helical conformation

(37) Rohl, C. A.; Scholtz, J. M.; York, E. J.; Stewart, J. M.; Baldwin, R. L. *Biochemistry* **1992**, *31*, 1263−1269.

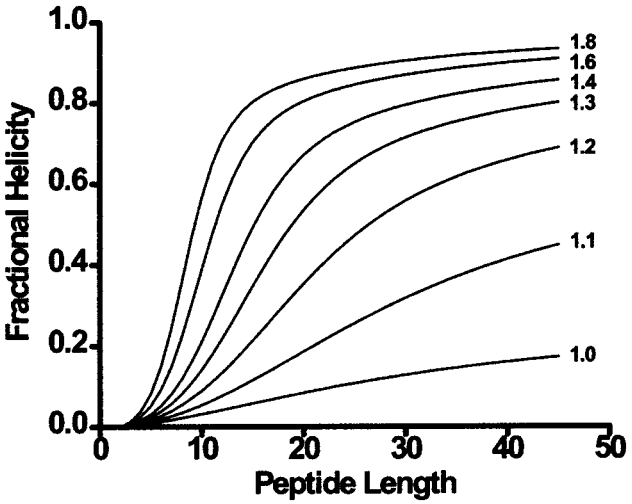

Figure 15. Fractional helicity plotted vs homopeptide length n for $v = 0.048$ and various values of w. The sigmoid shape exhibited for $w = 1.8$ is not evident at significantly lower values of w. Note that at a length of 12 residues there is a large difference between the expected helicity for the reported values of $w \approx 1.1$ and 1.6.

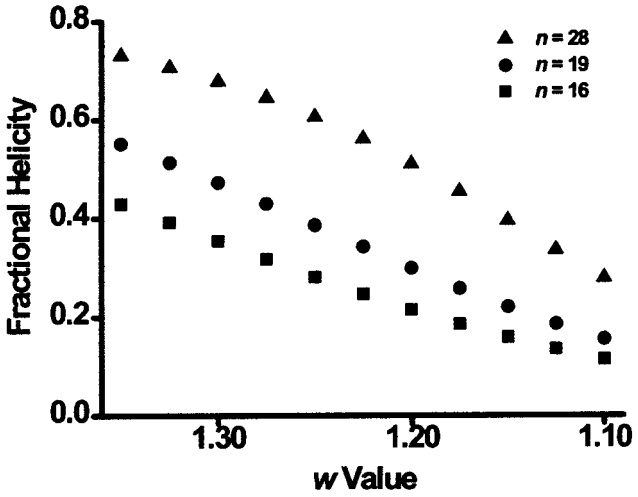

Figure 16. Fractional helicity plotted vs w for $v = 0.048$ and three different lengths $n = 16$, 19, and 28. This plot is qualitatively similar to that displayed in Figure 13, with the forms of the temperature dependences of A_{16} and A_{19}, which show upward curvatures, being significantly different from the form of the temperature dependence of A_{28}, which demonstrates downward curvature.

is increased by w, 49 new partially helical states are also added to the manifold. This balance between enthalpic and entropic stabilization effects causes helical fraying to stubbornly persist.

The interplay between the different molecular populations found in the three length-dependent regions is responsible for the characteristic sigmoid form of f_H vs n that is found for moderately large w and that is evident in Figures 14 and 15. If w is decreased, the width of region I increases, the slope of region II decreases, and the overall sigmoid form of the plot is less apparent. As w approaches 1.0, w^k can be approximated as $[1 + k(w - 1)]$, which increases only modestly with length. As seen in Figure 15, for this case no hint of sigmoid character is apparent.

A comparison of curve shapes in Figures 12 and 15 shows that the sigmoid length dependence seen for $[\theta]_{222}$ of the A_n series in water at 2 °C is strikingly similar to the modeling predictions for f_H using a w value of 1.3, and that w values in the range of 1.2 and 1.1 are plausible for the A_n data at 25 and 60 °C. The remarkable qualitative similarity of the plots of $-[\theta]_{222}$ vs temperature (Figure 13) and f_H vs w (Figure 16) provides confirmation of these tentative conclusions. In the next section these conclusions are tested more rigorously through L−R calculations that make use of plausible ellipticity functions.

Tests of Ellipticity Functions and Tentative Assignments of w_{Ala}. The most commonly used function[38,39] relating f_H to experimental $[\theta]_{222}$ has the form shown in eq 4, which defines

$$[\theta_n]_{222} = [\theta_\infty]_{222}\left(1 - \frac{x}{n}\right) \quad (4)$$

$[\theta_n]_{222}$, the residue ellipticity of an idealized 100% helical peptide of length n, in terms of two parameters, $[\theta_\infty]_{222}$, the limit of $[\theta_n]_{222}$ for very large n, and a length correction x. The latter has been assigned a range of values[39] but has been set[3a,40] at 2.5, and we use this value throughout this study. Fractional helicity is then estimated from observed values of $[\theta]_{222}$ by the usual approximation of eq 5.

$$[\theta]_{222} \approx [\theta_n]_{222} f_H \quad (5)$$

Ultimately the form of a rigorous ellipticity function and its internal parameters must be assigned from experimental $[\theta]_{222}$ data acquired for a series of model peptides of precisely known, high fractional helicity; such studies are currently in progress. In this report we test a literature ellipticity function and refine the value assigned to $[\theta_\infty]_{222}$, using minimization of the least-squares error shown in eq 6 as the criterion for goodness of fit.[41]

$$\sum \delta^2 = \sum (\text{calculated } [\theta]_{222} - \text{experimental } [\theta]_{222})^2 \quad (6)$$

Recently, Luo and Baldwin[42] introduced a form of eq 4 that sets $x = 2.5$ and $-[\theta_\infty]_{222} = 44\,000$ deg cm^2 dmol^{-1}, which defines an upper limit among the widely cited values for the latter parameter. We test this function against the 2 °C dataset of Figure 12, using w as the single variable parameter. A w-dependent database of f_H values was calculated from eq 3 for the 19-member A_n series, and this was converted to a $[\theta]_{222}$ database using both eqs 4 and 5. The minimized least-squares variance[41] $\sum \delta^2$ obtained by this fitting is 639, with an optimal w_{Ala} of 1.45. As seen by comparison of the data points of Figure 17 with this calculated $[\theta]_{222}$ (dotted line), the error in fit is very large, and the ellipticity function of Luo and Baldwin grossly underestimates $[\theta]_{222}$ data for n greater than 24 residues.

The failure of this modeling test can be attributed largely to the value of $-[\theta_\infty]_{222}$, which is clearly too small. It is equaled by the experimental values of $[\theta]_{222}$ for A_{44} and A_{45}, yet the L−R model predicts that each must be a frayed helix, with a f_H value less than 1.0. In a second modeling experiment (solid line in Figure 17) we treat both w and $-[\theta_\infty]_{222}$ as variable

(38) Chen, Y.-H.; Yang, J. T.; Chau, K. H. *Biochemistry* **1974**, *13*, 3350−3359.
(39) Gans, P. J.; Lyu, P. C.; Manning, M. C.; Woody, R. W.; Kallenbach, N. R. *Biopolymers* **1991**, *31*, 1605−1614.
(40) Scholtz, J. M.; Qian, H.; York, E. J.; Stewart, J. M.; Baldwin, R. L. *Biopolymers* **1991**, *31*, 1463−1470.
(41) The error reported herein is based on data of the form $[\theta]_{222} \times 10^{-3}$ deg cm^2 dmol^{-1}.
(42) Luo, P.; Baldwin, R. L. *Biochemistry* **1997**, *36*, 8413−8421.

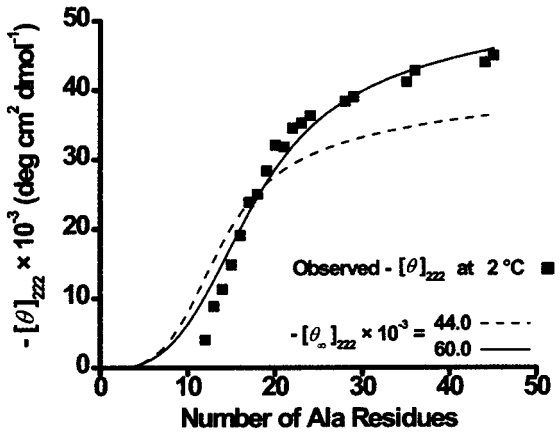

Figure 17. Results of mathematical fitting of the polyalanine $[\theta]_{222}$ data at 2 °C. The dashed line clearly demonstrates that the assignment of $-[\theta_\infty]_{222} = 44\,000$ deg cm^2 dmol^{-1} is inappropriate, yielding a w value of 1.45 with $\sum\delta^2 = 639$. Fitting the data while allowing $-[\theta_\infty]_{222}$ to vary yields for this parameter a value of 60 040 deg cm^2 dmol^{-1} and produces a much better fit of the experimental data, with $\sum\delta^2 = 115$. Using this simple Lifson−Roig model, the value of w_{Ala} at 2 °C is 1.31.

parameters, obtaining optimal respective values of 1.31 and 60 040 deg cm^2 dmol^{-1}, with a substantially improved $\sum\delta^2$ variance of 115.

This assignment of $-[\theta_\infty]_{222} = 60\,040$ finds independent precedent in two of our recent investigations, which report $-[\theta_\infty]_{222} = 61\,000$, within experimental error of the present assignment. One study examined highly helical Ac-Hel conjugates of Baldwin−Marqusee $(A_4K)_x$ peptides in the size range 17−27 residues in water at 2 °C.[35] The other used t/c-derived fractional helicities to assign an optimal $-[\theta_\infty]_{222}$ to spaced, water solubilized, N-templated polyalanines in the series Ac-Hel-$A_n{}^tLInp_2K_4WNH_2$, $2 \le n \le 14$.[13] The consistency between all three independent studies is suggestive. Although rigorous assignment of $[\theta_\infty]_{222}$ still awaits further confirmation from independent experiments that are in progress, for the interim we adopt a value of 61 000 deg cm^2 dmol^{-1} for $-[\theta_\infty]_{222}$ as a working hypothesis for the analyses in this report.

Modifications to the Standard Lifson−Roig Modeling. Inspection of Figure 17 shows that the fit between the data points and the solid curve is not perfect, as the curve underestimates $[\theta]_{222}$ for peptides in the length region 19−24 residues and overestimates it for shorter peptides. As a consequence, the experimental slope of the graph between 12 and 24 residues is significantly larger than the calculated value. In this section we examine in turn three features implicit in the L−R ellipticity calculation of the preceding section that may contribute to this fitting problem. We conclude the section by modifying the L−R algorithm to correct for each feature; we then show that this new algorithm provides a fit within the experimental error of the data.

Appropriate Usage of the Ellipticity Function. Though widely used, eq 5 only approximates a true value of $[\theta]_{222}$ since it applies to all of its partially helical conformations, short or long, a single ellipticity constant $[\theta_n]_{222}$ appropriate only for the completely helical conformation of the peptide. This approximation creates internal inconsistencies in $[\theta_k]_{222}$ for short helical conformations that appear in peptides of different lengths; a three-residue helical conformation that appears within the manifold of A_{45} is assigned a larger ellipticity than the same conformation in the A_{12} manifold. Using eq 5 thus slightly overestimates any $[\theta]_{222}$ assigned to a short peptide; depending on w the effect can be as high as 5% for an A_{12} peptide. A self-consistent expression for calculated L−R $[\theta]_{222}$ is given by eq 7. In this expression the calibration function eq 4 is used

$$[\theta]_{222} = \sum [\theta_k]_{222} \frac{k}{n} \chi_k \qquad (7)$$

implicitly, setting $n = k$ to calculate the partial residue ellipticity for each conformation that contains a helical region of length k. A 10% improvement in $\sum\delta^2(115 \rightarrow 105)$ is obtained when the solid line of Figure 17 is recalculated after replacement of eqs 3 and 5 by eq 7, and in this fit the value of w is slightly greater (1.31 → 1.33).

Helix Capping Corrections. As noted earlier, a rigorous L−R ellipticity calculation for spaced, solubilized A_n peptides must employ capping corrections for the pair of ^{t}L functions that terminate the alanine core region. If these caps destabilize the helix, their effects are expected to be greatest for short helices. Numerical values of relative capping propensities have been proposed.[21] We have recently rationalized capping effects and introduced data[43] that allow calculation of the relative C-capping propensity of ^{t}L at 2 °C as 0.77. Because the mechanism of the effect is likely to be similar, we also use this value for the relative N-capping propensity of ^{t}L. The ellipticity algorithm used in the calculation of the preceding paragraph was further modified to include these capping parameters, yielding $w = 1.34$, again with a 10% improvement in $\sum\delta^2$ (105 → 94), but with no qualitative change in the systematic deviations found in the central region of Figure 17.

The Cooperativity Model. We retain the features of the two modest improvements probed in the above sections in devising an algorithm that addresses a more significant effect. Recently we proposed a fundamental revision in the L−R algorithm that assigns special parameters to very short helical conformations,[13] which hitherto have been difficult to study. The need for new parameters arose from investigation of the t/c and ellipticity properties of the series Ac-Hel $A_n{}^tLInp_2K_4WNH_2$, $2 \le n \le 14$, in which the polyalanine sequence is N-capped by the helix initiating and reporting Ac-Hel. The unique properties of Ac-Hel permit characterization of helices formed by very short peptides, which show temperature dependences, intrinsic helicities, and CD intensities that are significantly different from those of longer helices. To explain these differences, we invoked hydrogen-bonding cooperativity. Theory has predicted an increase in amide−amide hydrogen bond strength when chains of intramolecularly H-bonded secondary amides are extended.[44] For helical conformations in the length range of 3−16, the effect of such cooperativity is to make w values dependent on the length of a helical conformation. We successfully modeled both t/c and CD data for the above series using the following assumptions. For $n < 5$, w is set at 1.0, but for longer helices w is treated as a free parameter. The ellipticity function using $x = 2.5$ and $-[\theta_k]_{222} = 61\,000$ is adopted for $k > 8$, but $-[\theta_k]_{222}$ is set at 53 000 for $k \le 8$ to accommodate calibration data at $n = 8$ for a highly helical peptide.[13]

(43) Maison, W.; Kennedy, R. J.; Miller, J. S.; Kemp, D. S. *Tetrahedron Lett.* **2001**, *42*, 4975−4977.
(44) (a) Guo, H.; Karplus, M. *J. Phys. Chem.* **1992**, *96*, 7273−7287. (b) Guo, H.; Karplus, M. *J. Phys. Chem.* **1994**, *98*, 7104−7105. (c) Kobko, N.; Paraskevas, L.; del Rio, E.; Dannenberg, J. J. *J. Am. Chem. Soc.* **2001**, *123*, 4348−4349.

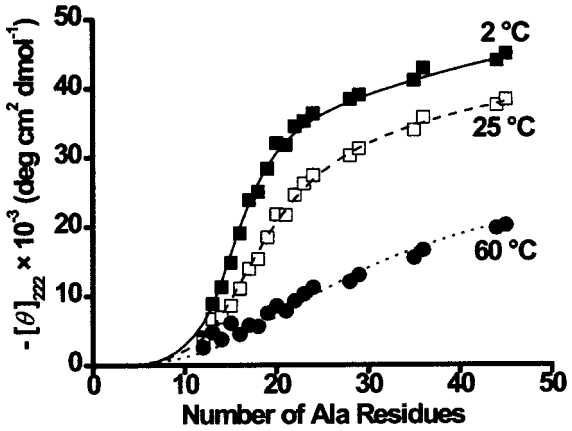

Figure 18. Results of mathematical fits using the new cooperativity model for the polyalanine $[\theta]_{222}$ data at 2, 25, and 60 °C. Altering only two temperature-dependent parameters w and z, one obtains excellent fits at each temperature. The curvature of the data in all three regions of each plot is faithfully reproduced by the modeled values. The fit at 2 °C yields values for $w_{Ala} = 1.27$ and $z = 1.41$ with a total error $\sum\delta^2 = 16$; at 25 °C $w = 1.18$ and $z = 1.34$, with $\sum\delta^2 = 9.2$; at 60 °C $w = 1.06$, $z = 1.16$, and $\sum\delta^2 = 24$.

In applying this function to the spaced, solubilized A_n series a new cooperativity parameter is added to the L−R algorithm to account for a possible length discrepancy. The longest A_n region of the Ac-Hel-A_n^{t}LInp$_2$K$_4$WNH$_2$ series cannot be extended beyond 14 residues,[13] allowing only a two-point overlap with the A_n length series of the present study. To allow for further H-bonding cooperativity beyond the length range of 12−14 residues that could not be detected through our analysis of the Ac-Hel series, a new cooperativity parameter z is introduced here. A weight of z^3w^k is assigned to helical conformations of length $k = 15$ or longer; to allow a smooth mathematical transition,[45] helical conformations of 12−14 residues in length are assigned weights $z^{(k-11)}w^k$.

This modified L−R algorithm using our composite ellipticity function (eq 7) was applied to $[\theta]_{222}$ data for the A_n series at each of the three temperatures 2, 25, and 60 °C to yield best fit, temperature-dependent values for w and z. From these, the three fits for length-dependent $[\theta]_{222}$ displayed in Figure 18 were calculated, yielding the values for w, z, and $\sum\delta^2$ listed in the figure legend. At the three temperatures of the study, calculated values of $[\theta]_{222}$ fit the observed ellipticities within their experimental precision.

Summary of Modeling Results

At any one temperature the fit of Figure 18 has been achieved by a plausible model containing only two free parameters. A comparison between the values of w assigned by this study and by our previous modeling of the Ac-Hel-A_n^{t}LInp$_2$K$_4$WNH$_2$ series reveals their consonancy. For the latter series we assigned w values of 1.29 at 2 °C and 1.215 at 25 °C; from our present study, the corresponding values are 1.27 and 1.18. A parameter w derived from study of A_n peptides of maximum length 14 and bearing the Ac-Hel N-cap corresponds within the error of assignment to the w value assigned to a series of spaced, isolated A_n peptides that extends to 45 residues.

Our ellipticity function still contains primitive features, but given the consistency of the above modeling results, it may approximate a rigorous function that is tailored for alanine-rich peptides. This function is markedly deviant from those optimized for the study of globular proteins or peptides whose composition is dominated by amino acids other than alanine.[46] The causes of that deviation are currently speculative and await further experimental study. It is also premature to regard the 86% reduction in $\sum\delta^2$ seen for the 2 °C $[\theta]_{222}$ data as rigorous validation of our cooperativity model. What can be concluded is that for the first time a single helicity model and ellipticity function have been shown to quantitatively reproduce the helical properties of short templated alanine helices as well as the first complete length series of solubilized, charge-isolated polyalanines.

Conclusion

We have also measured the first intrinsic helical propensities of alanine in a polyalanine context and found that more than one parameter is required for a best fit to the experimental data. Previous w values proposed for alanine by the Scheraga and Kemp groups have upper limits in the range of 1.07−1.15. These are consistent with the values we have found for very short alanine peptides.[13] The w values proposed by Baldwin, Stellwagen, Kallenbach, and their co-workers lie in the range of 1.6−1.9, and are inconsistent with our modeling data, for which a maximum w value for alanine in water must lie in the vicinity of 1.3. Probable causes of this discrepancy will be discussed in subsequent reports. A conclusive test of the appropriateness of our new w values awaits a rigorous calibration of the ellipticity function, further confirmation of our H-bonding cooperativity model, and proof that the alanine helical propensities we have observed in a polyalanine context also apply to alanine within normal peptide sequences.

Experimental Section

Reagents. All purchased chemicals were used as received. Chemicals were purchased from the following suppliers: amino acids (AAs) and their derivatives from Novabiochem; biosynthesis grade *N*,*N*-dimethylformamide (DMF), high-performance liquid chromatography (HPLC) grade methanol, and anhydrous diethyl ether from EM Science; trifluoroacetic acid (TFA) from Advanced ChemTech; HPLC grade acetonitrile from Mallinckrodt; 1,8-diazabicyclo[5.4.0]undec-7-ene (DBU), piperidine, and diisopropylethylamine (DIEA) from Aldrich or Alfa Aesar, interchangeably; [*O*-(7-azabenzotriazol-1-yl)-1,1,3,3,-tetramethyluronium hexafluorophosphate] (HATU) and polystyrene (PS) functionalized with poly(ethylene glycol) (PEG) and PE Biosystems' peptide amide linker (PAL) from PerSeptive Biosystems (PE Applied Biosystems). Water was purified and deionized to 18.2 MΩ using a Millipore Gradient A10 water purification system equipped with a total organic carbon (TOC) monitor reading under 5 parts per billion (ppb).

Solid-Phase Synthesis. Peptides were prepared on a 0.025 mmol scale by automated continuous-flow solid-phase synthesis on a PE Biosystems Pioneer peptide synthesizer using standard 9-fluorenylmethoxycarbonyl (Fmoc) chemistry. Fmoc-AAs (≥3 equiv) were weighed into labeled, letter-coded, 13- × 100-mm test tubes;[47] HATU (≤3 equiv, ≤28.5 mg) was then added to each test tube.[48] After the test tubes were placed in the appropriate racks, PAL-PEG-PS resin (0.17

(45) See Supporting Information for a detailed explanation of these cooperativity weighting assignments.

(46) Besley, N. A.; Hirst, J. D. *J. Am. Chem. Soc.* **1999**, *121*, 9636−9644.

(47) Precision is not required for weighing out reagents; equivalents reflect averages over tens or hundreds of test tubes prepared at one sitting, with randomly selected test tubes each within the stated limits.

(48) The number of equivalents of HATU must be fewer than the number of equivalents of Fmoc-AA to avoid sequence capping by a terminal guanidium ion, see: Albericio, F.; Bofill, J. M.; El-Faham, A.; Kates, S. A. *J. Org. Chem.* **1998**, *63*, 9678−9683 and references therein.

mequiv/g, ~150 mg) was weighed into a synthesis column and washed with methanol. DMF was washed through the column on the synthesizer at a flow rate of 30 mL/min while the resin was compressed and released by successive tightening and loosening of the column to remove bubbles and swell the resin. When no air bubbles remained (about 1 min, with gentle tapping when the resin was not compressed), the column was tightened to accommodate only the volume of the swollen resin, and the flow of DMF was stopped. Fmoc removal (deblock) was accomplished using a 1:1:48 (v:v:v) mixture of DBU:piperidine:DMF[49] for 6 min at a flow rate of 6 mL/min directly to waste and was monitored by integrating over time the UV absorbance of cleaved Fmoc chromophore. Each coupling step involved the reagents in a single test tube and excess DIEA in DMF for 30−60 min at a recycling flow rate of 30 mL/min. Multiple successive washes of DMF and methanol were used to prepare the growing resin-bound peptide for successive steps. The final deblocked peptide was washed out of the synthesis column with methanol into a manual peptide synthesis vessel and dried in vacuo.

Peptide Cleavage. Peptides were cleaved with 7 mL of a cocktail[50] prepared directly before usage consisting of approximately 83% TFA, 5% phenol, 5% water, 5% thioanisole, and 3% 1,2-dithioethane (all by volume) for 2 h under an argon atmosphere and precipitated by dropwise addition to 35 mL of cold dry diethyl ether in a 50-mL polypropylene (PP) conical tube immersed in a dry ice−acetone bath. The cold ether slurry was allowed to warm to room temperature[51] over 30 min, at which time it was placed in a centrifuge and spun at 3.5×10^3 revolutions per minute (krpm) for 8 min. The precipitate was washed three times with ether. Each time the supernatant was decanted and the conical tube closed and vortexed for <1 min, until the solid clump loosened.[52] Ether at room temperature was then added (20 mL), the tube reclosed, and the suspension vortexed for a short time and placed back in the centrifuge for 8 min. After decanting of the final wash, the conical tube was closed halfway, and the peptide was placed under vacuum and dried at least 10 min. The crude, pale brown or white solid peptide was dissolved in 18.2 MΩ water and purified by HPLC.

Preparative and Analytical HPLC. Preparative HPLC separations were performed on a Rainin Dynamax SD-200 system equipped with a two-channel (set at 214 and 280 nm) Rainin Dynamax UV-D II detector and Rainin Dynamax HPLC Method Manager software. Analytical HPLC separations were performed using a Waters 490 programmable multiwavelength detector with a Waters 600E system controller and a Waters 746 data module. All separations involved a mobile phase of 0.05% TFA in water (solvent A)/0.042% TFA in acetonitrile (solvent B). HPLC output was monitored at 214 and 280 nm.

Crude separations were performed using a Waters DeltaPak C_{18} 300-Å, 19- × 300-mm stainless steel column equipped with a short, hand-packed C_{18} (EM Science) guard column. For a typical crude separation (to remove non-peptidic material), the column was allowed to equilibrate at 5%B and 16 mL/min for 7 min, at which time crude peptide (10−25 mg) in 4.5 mL of water was taken up in a 5-mL syringe and injected onto the column. The solvent gradient ran at 16 mL/min from 5%B (initial) to 50%B at a ramp of 3%B per minute (15 min), then to 95%B over 1 min and held at 95%B for an additional 6 min.[53] Peptides usually eluted in a span of 30−60 s (a volume of 8−16 mL).

Analytical HPLC characterization was then performed using a YMC ODS-AQ 200-Å, 4.5- × 150-mm stainless steel column equipped with a similarly packed 4.5- × 20-mm guard column. Analytical gradients run at 1 mL/min started at 5%B, jumped over 1 min to *x*%B, then to (*x* + 10)%B at 1%B per minute (10 min), then to 95%B over 1 min, and held at 95%B for 5 min. The parameter *x* was chosen on the basis of crude purification to elute the peptide at about 7 min into the 10 min gradient at 1%B per minute.[54] The peak shape on this system using these parameters was excellent, affording nearly baseline separations between the solubilized polyalanines and their lysine or alanine deletion sequences (as checked by MS). Figure 19, which plots the elution percentage of solvent B on this system against the number of alanine residues in the polyalanine conjugates, demonstrates the fact that the peptides are separable.

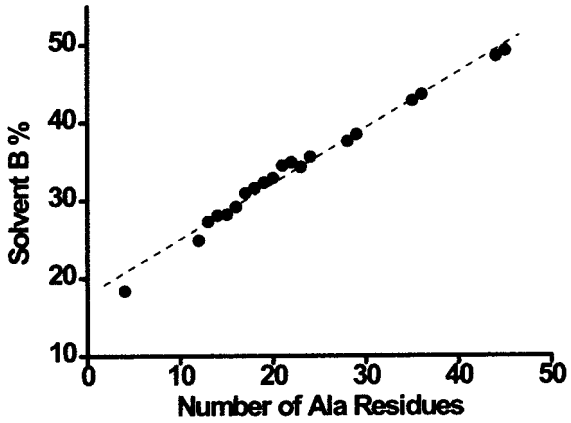

Figure 19. Solvent B elution percentage vs the number of alanine residues *n* in peptides of the form $WK_mInp_2{}^tLA_n{}^tLInp_2K_mNH_2$, $m = 4-6$. Homoalanines differing in length by only one alanine residue were separable by HPLC in every case using a YMC ODS-AQ 200 Å column. The dashed line indicates a linear fit (%B = 0.176*n* + 17.9) of the data with an *R* value of 0.9924.

Fine preparative separations were accomplished using a YMC ODS-AQ 200-Å, 10- × 150-mm stainless steel column equipped with a similarly packed 10- × 20-mm guard column. Eluent from the crude purification was injected in two batches (<10 mL each) onto the column, each eluted at 16 mL/min using the same gradients as those used in the analytical run. Peak shapes were broad and irregular on the preparative column due to sample overloading, but compound separation was good. Pure peptide eluted over 60−90 s for each run (32−48 mL total) was collected in a clean 50-mL PP conical tube. The criteria for purity were a single, symmetrical peak when rechecked by analytical HPLC and an ultraviolet spectrum (see below) between 250 and 300 nm showing the normal characteristic peak shape of the W chromophore with a maximum at 279 nm and two distinct shoulders on either side. Purified peptides were lyophilized, transferred to 15-mL tared PP conical tubes, and then lyophilized twice from 18.2 MΩ purified water and stored as white solids at room temperature for short periods of time or in PP conical tubes at or below 0 °C for extended periods. Solutions of the peptides (see below) were also stored frozen in PP conical tubes.

Characterization. CD and UV Spectroscopy. CD experiments were performed on an Aviv 62DS spectrometer equipped with a thermoelectric temperature controller and an Osram XBO 450-W high-pressure xenon lamp. CD data were collected after a 12-min temperature

(49) Kates, S. A.; Solé, N. A.; Beyermann, M.; Barany, G.; Albericio, F. *Pept. Res.* **1996**, *9*, 106−113.
(50) Precision was again found not to be a factor. Solid phenol was added to a 15-mL PP conical tube up to the 1.5-mL mark; thioanisole and 1,2-dithioethane were added (~2:1) to about the 2-mL mark; 5−7 drops of 18.2 MΩ water from a pipet were added; TFA was added to about the 14−15-mL mark. The conical tube was closed and inverted 20 times, or until no solid phenol remained. The resulting clear, colorless solution was split and used to cleave two peptides.
(51) Precipitate sometimes formed only upon warming.
(52) The more highly charged peptides tended to yield more clumpy precipitates at this stage. After 1 min of vortexing, the wash was simply continued as indicated.
(53) Dwell volume on this system led to a time lapse of approximately 2.5 min between injection and elution of the first solvent front. The gradient delay time was about 5 min, meaning a change in gradient took min to reach the detector. Peptides invariably eluted before the 6 min at 95%B expired, except for the most hydrophobic cases, for which the 3%B gradient was extended.
(54) Dwell volume on this system led to a delay of approximately 1.5 min between injection onto the column and elution of the solvent front. A broad "peak" commensurate with a sudden change in mobile phase composition starting at low %B is produced with this solvent system. This peak was used to determine the gradient delay time of about 6 min (from the initial injection to the elution of the middle of the 1%B per minute gradient), giving an ideal elution time of about 13 min.

equilibration as an average of five scans at 1.0-nm bandwidth and 0.5-nm step size. After blank correction, spectra were smoothed using Aviv 62DS version 4.0s software polynomial fitting; high-wavelength (250−255 nm) ellipticities were close to zero and were therefore left uncorrected. UV spectroscopy was performed on a double-beam Varian Cary 100 Bio UV−visible spectrometer. Single-wavelength UV data were taken as an average of five scans. UV and CD cells (Hellma, QS, strain-free suprasil) were cleaned prior to each use first with water, followed by drying under vacuum, then with concentrated sulfuric which was drained without dilution, then again with purified water, followed again by drying under vacuum. The outsides of the windows were then wiped with HPLC grade methanol immediately prior to placement in the spectrometer. Solvent blanks for UV and CD scans were taken immediately prior to use of each cell by using two clean 10-mm cells (in the double-beamed UV spectrometer) containing ~3.5 mL of the appropriate solvent. After a full UV scan (190−340 nm) was taken indicating no contamination, five scans at 280 nm were taken. The cell used for baseline correction (in the second compartment of the double-beamed spectrometer) was left in the UV spectrometer while blank scans of the sample cell were taken on the CD. The sample cell was then removed, rinsed (if buffer other than pure water was used), dried in a vacuum, and filled with ~3.5 mL of CD sample prepared as described below. Concentration was determined by the UV absorption of tryptophan[15] with $\epsilon_{280} = 5.56 \times 10^3\ M^{-1}\ cm^{-1}$ (see Appendix). After a full UV scan of the CD sample (190−340 nm) was taken, five UV scans at 280 nm were taken. CD spectra were then obtained as indicated.

Solution Preparation. Solutions were prepared with the goal of obtaining consistent concentrations for CD measurements as determined for each CD sample by using the tryptophan chromophore ϵ_{280} (see Appendix). Solid peptides were prepared by lyophilizing from water entire samples of purified peptides in 15-mL PP conical tubes. Peptide stock solutions were then prepared by dissolving the lyophilized peptides in ~10 mL of the appropriate solvents. Following concentration determination using the tryptophan ϵ_{280}, the stock solutions were diluted (by mass) to concentrations appropriate for CD (7−15 μM) with purified water or buffer by the following procedure. To a new, tared, 15-mL PP conical tube was added about 0.5 g of peptide stock solution; the exact mass of the added stock solution was recorded. Purified water or buffer was then added, usually between 5 and 12 mL (depending on the concentration of the stock solution), to reach the desired dilution; the total mass of diluted solution was recorded.

Some solutions were prepared by lyophilizing CD samples (in purified water only) and redissolving in the appropriate buffer. In all cases, CD sample concentrations were determined by UV measurement of ϵ_{280} for tryptophan directly before CD measurements were taken.

Mass Spectroscopy. Electrospray mass spectroscopy (ESMS) of CD samples in pure water taken on a Waters Micromass ZMD 4000 yielded mass-to-charge (m/z) ratios within 0.75 mass unit of the expected values and in each case showed several peaks corresponding to a range of values of z for a single value of m.

Analytical Ultracentrifugation. Analytical ultracentrifugation data were obtained on a Beckman Optima XL-A centrifuge using an An-60 Ti analytical rotor and a six-channel centerpiece. For experimental details, see Supporting Information.

Acknowledgment. We thank Professor Robert Sauer for providing access to his ultracentrifuge. Generous financial support is acknowledged from NIH Grant GM13453, NSF Grant 9727356-CHE, and Pfizer Research.

Appendix. Tryptophan Extinction Coefficient at 280 nm

Introduction. Concentration determination of a dilute sample of a polypeptide in water can be a large source of experimental error in the calculation of peptide $[\theta]_{molar}$. While several methods have been employed previously, the use of ultraviolet chromophores such as the natural amino acids tyrosine (Y) and tryptophan (W) has become common due to the convenience and potential accuracy of the method. Though it has been observed that inclusion of a UV chromophore close to a helical region in a peptide can have unpredictable and therefore undesirable effects on the $[\theta]_{molar}$ exhibited by the peptide, isolation of the chromophore from the helical region alleviates this problem.[14,55] Variations in local (intrapeptide) or global (buffer) ionic strength or other contexts might also affect the extinction coefficients of the heteroaromatic or heterosubstituted aromatic $\pi \rightarrow \pi^*$ transitions exhibited by these amino acid residues.[56] Unfortunately, while the literature values for extinction coefficients of simple chromophores used for concentration determination[15] take into account potential dependences such as pH, they do not necessarily take into account all appropriate potential context dependences of the chromophores. Literature protocols for concentration determination often require UV absorbance measurements either in denaturing conditions (6.0 M guanidine hydrochloride) or by serial dilution of a concentrated sample or both. Such protocols are obviated by the solubilizing, spacing nature of the peptides introduced in this report combined with an appropriate calibration method for the absorbance of the tryptophan chromophore in this local peptide context at CD concentrations. The goal of this study is to determine whether ϵ_{280} previously reported for the tryptophan chromophore applies to a W residue in the local context of the solubilized, spaced polyalanines reported here.

Design. Assigning the extinction coefficient of tryptophan requires multiple measurements that allow cross correlation of ϵ values. Such calculations demand aqueous solutions for UV assays containing W derivatives at precisely defined concentrations. The obvious method involves preparation of primary UV calibration standards in the form of crystalline simple tryptophan derivatives of proven purity. For this we used free tryptophan and its amide hydrochloride; both are easily purified by recrystallization and can reveal the baseline behavior of the W chromophore lacking any local peptide contexts. Solutions of known concentrations of these primary standards were prepared and subjected to UV measurements, yielding ϵ_{280} in three solvent contexts: purified, deionized (18.2 MΩ) water, aqueous 100 mM sodium chloride, and aqueous 6 M guanidine hydrochloride (GuHCl). This is the classical method for assigning ϵ values, and it has the virtue of simplicity, but complex peptides containing W residues at their solubilized, spaced N-termini cannot be used as primary standards since such peptides are noncrystalline and, like all peptides, tenaciously retain traces of water or inorganic salts. Their weights are therefore unreliable measures of their molar quantities. Our second tactic involved preparation of aqueous solutions that in addition to the test tryptophan peptide derivative contained known amounts of a simple crystalline organic molecule that could be used as a primary standard. The organic molecule was selected to maximize a comparison of its concentration with that of the W peptide derivative by nuclear magnetic resonance (NMR)

(55) (a) Freskgård, P.-O.; Mårtensson, L.-G.; Jonasson, P.; Jonsson, B.-H.; Carlsson, U. *Biochemistry* **1994**, *33*, 14281−14288. (b) Andersson, D.; Carlsson, U.; Freskgård, P.-O. *Eur. J. Biochem.* **2001**, *268*, 1118−1128 and references therein.
(56) Brandts, J. F.; Kaplan, L. J. *Biochemistry* **1973**, *12*, 2011−2024.

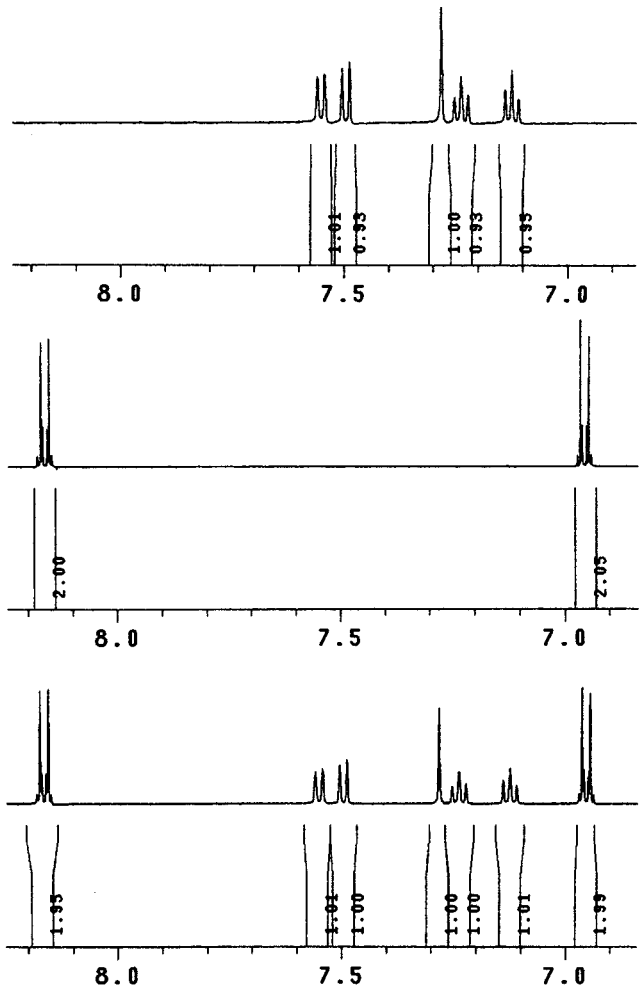

Figure 20. Aromatic regions of NMR spectra of solutions containing a peptidic tryptophan derivative (top), *p*-nitrophenol (middle), and both (bottom). Well-suited as an internal standard for NMR integration with tryptophan-containing peptides, *p*-nitrophenol is easy to purify and handle, and it has NMR properties similar to those of the reporting W chromophore.

integration using a relaxation delay time of sufficient length to avoid errors associated with differential T_1 relaxation.

The simplest usable NMR peaks associated with our solubilized polyalanines are the aromatic resonances arising from the tryptophan UV chromophore itself. However, the commonly employed internal standard, sodium 3-(trimethylsilyl)propionate-*2,2,3,3-d*$_4$ (TMSP), exhibits NMR resonances far upfield, beyond even the normal aliphatic region. Comparison of the W and TMSP peaks cannot under most circumstances be expected to give by peak integration an accurate correlation between the relative concentrations of the two species in solution. Instead, we introduced a new internal standard, *p*-nitrophenol.

p-Nitrophenol has distinct advantages over TMSP as an internal standard for our NMR concentration measurements. Its aromaticity makes it much more comparable to the W chromophore in chemical structure than the previous standard; in fact, as illustrated in Figure 20, the aromatic resonances of W fall between 7.1 and 7.8 ppm and the resonances of *p*-nitrophenol occur at 6.95 and 8.17 ppm, directly on either side of—but not overlapping with—the W resonances. Also, *p*-nitrophenol is particularly easy to purify and handle, as it is easily sublimed, yielding a crystalline solid insensitive to air and water, and it is quite soluble in water.

With tryptophan derivatives at known concentrations determined by a method described above, a calibration of the tryptophan ϵ_{280} for these W derivatives at CD concentrations was undertaken. Conventionally, spectrometric concentration assays are most accurate if the chromophore concentration and cell length yield an experimental absorbance ranging from 0.3 to 0.7. Using the simple tryptophan primary standards, we began by making measurements at these concentrations, but we then extended them to the optical density region characteristic of solutions used in CD measurements, typically in the micromolar concentration range. The success of this tactic clearly depends on the accuracy and reproducibility of the UV spectrometer used in the study. It also requires careful and consistent preparation of UV sample cells. Because the W chromophore at CD concentrations requires measurements near absorbances of 0.1, we calibrated our double-beam Varian Cary 100 Bio UV−vis spectrometer to 0.05 absorbance unit and determined that such measurements clearly lie within the capabilities of the instrument (see Supporting Information). The typical specification of ±0.00016 absorbance unit using the double aperture method corresponds to a 0.3% error of measurement at these concentrations of the W chromophore. The instrument demonstrated excellent reproducibility between scans regardless of whether the sample cell was removed and replaced or simply left in the cell compartment.

Materials. We used two methods for checking purity as indicated below; our use of elemental analyses deserves special comment. A reliable method for demonstrating amino acid purity especially from the likely impurities of water and inorganic salts is through an assay of nitrogen content, because neither of these impurities contains nitrogen. Thus, the appropriate values listed below obtained for nitrogen composition indicate a high degree of purity. It is also useful to compare elemental analysis results to the expectations for oxygen content, as this is not generally determined directly, but by difference. Accurate oxygen content thus measured provides good evidence for purity from any inorganic materials that do not contain significant percentages of carbon, hydrogen, and nitrogen.

Deuterium oxide (D, 99.9%) was used as received from Cambridge Isotope Laboratories, Inc. GuHCl and NaCl from Mallinckrodt were used as received. Criteria for peptide purity were as noted earlier.[11] Purity of crystalline tryptophan derivatives was checked by the Karl Fischer test for water (KF) and by two combustion analyses each, showing an error of ±3%. H-Trp-OH from Novabiochem was recrystallized as white plates from a dilute solution of ethanol in water and dried in vacuo to a constant mass. KF test showed less than 0.10% water by mass. Anal. Calcd for $C_{11}H_{12}N_2O_2$: C, 64.69; H, 5.92; N, 13.72; O, 15.67. Found: C, 64.60; H, 5.76; N, 13.72; O (by difference), 15.92. H-Trp-NH_2·HCl from Novabiochem was dissolved in boiling ethanol and then recrystallized as small, off-white feathers from ethanol−ethyl acetate (5:1) and dried to a constant mass. KF test showed 0.30% water. Anal. Calcd for $C_{11}H_{14}N_3ClO$: C, 55.12; H, 5.89; N, 17.53; Cl, 14.79; O, 7.24. Found: C, 54.90; H, 5.82; N, 17.50; Cl, 14.54; O (by difference), 6.67. *p*-Nitrophenol from Aldrich (greenish brown) was sublimed and collected as very pale yellow needles. KF test showed <0.1% water. Anal. Calcd for $C_6H_5NO_3$: C, 51.80; H, 3.62; N, 10.07; O, 34.51. Found: C, 51.74; H, 3.50; N, 9.85; O (by difference), 34.91.

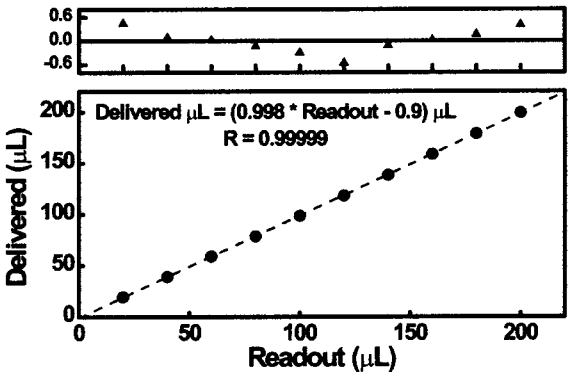

Figure 21. Graph depicting calibration of the micropipet used for delivery of all small volumes in this study. The fitted equation (dashed line) shown in the graph was used in conjunction with the pipet read-out to obtain precisely known volumes.

Procedures. The analytical balance (Sartorius Research) used was calibrated by Mettler-Toledo, Inc. Balances and Instruments within a week prior to the beginning of this study.

(i) Solution Preparations. To a washed, rinsed (deionized water), oven-dried, 100-mL volumetric flask cooled to room temperature was added freshly sublimed *p*-nitrophenol (0.1070 g, 0.7692 mmol). D_2O was added up to the 100 mL mark, and the flask was capped and inverted repeatedly until the yellow solution was completely mixed. The *p*-nitrophenol standard solution (7692 μM) was stored in two 50-mL PP conical tubes. Stock solutions of peptides were prepared by first lyophilizing pure peptides twice from D_2O and then dissolving the deuterated peptides in 3−5 mL of D_2O. Stock solutions of recrystallized solids were prepared by dissolving 1.000 ± 0.002 mmol of solid to a volume of 50 mL with H_2O in a 50-mL volumetric flask.

(ii) Micropipet Calibration. To ensure proper delivery of small volume samples with a micropipet, a single instrument (from Eppendorf Research) was used for every sample preparation in this study. The instrument was calibrated with results as indicated in Figure 21. The technique of touching the bead of liquid but not the pipet tip to the target vessel was employed throughout the study, including during calibration. After setting the micropipettor to deliver a specific volume, the actual volume delivered using this technique was recorded; the procedure was repeated a total of four times for each volume setting calibrated. The mass of water delivered was measured on an analytical balance; the ambient temperature was determined by averaging the read-outs of four thermometers. Volume was calculated from the recorded masses using the density of water at the ambient temperature.

(iii) NMR Measurements. The concentrations of stock solutions of the following peptides were determined by NMR: $WK_mInp_2^tLA_4^tLInp_2K_m$, $m = 2-7$, and $WK_4Inp_2^tL$. NMR solutions were prepared by adding to an NMR tube (Wilmad 535) 600 μL of peptide stock solution and 100.1 μL of *p*-nitrophenol standard solution followed by vigorous shaking. NMR spectra were obtained on a Varian Inova-500 MHz spectrometer with a relaxation delay time (d1) of 15.0 s, 90.0 deg pulse, 3.277 s acquisition time, and 10 000 Hz spectral width.

(iv) UV Absorbance Measurements. Single-wavelength UV data were taken as an average of five scans. UV and CD cells (Hellma, 1 cm, QS, strain-free suprasil) were cleaned prior to each use first with water followed by drying under vacuum, and then with concentrated sulfuric acid, which was drained without dilution, then again with purified water followed by drying under vacuum. The outsides of the windows were then cleaned with lintless wipes using HPLC grade methanol immediately prior to placement in the spectrometer. Blank UV scans with the appropriate solvents were taken immediately prior to use of each cell: to two clean cells (1 cm path length) was added ~3.5 mL of pure solvent. After taking a full UV scan (190−340 nm) indicating no contamination, five scans at 280 nm were taken. All cells were checked for the appearance of visible bubbles both before and after every UV (or CD) scan.

Dilute solutions for UV absorbance measurements were prepared as follows. Volumetric flasks were cleaned and rinsed with purified, deionized water and then oven-dried and cooled to room temperature (~21.0 °C). For stock solutions containing recrystallized solutes, 50−125 μL of a 20.00 mM stock solution transferred via pipet into an appropriately sized volumetric flask (5−50 mL) was diluted with either purified, deionized water, aqueous 100 mM NaCl or aqueous 6 M GuHCl and then inverted until completely mixed, giving for both solutes 10 solutions for each buffer in the range of 10−500 μM. Each peptide stock solution was diluted once from 99.9 μL to 10 mL and three times from 50 μL to 5 mL (four solutions, total) with purified, deionized water and mixed in a similar manner. All solutions were transferred to and stored in PP conical tubes immediately after mixing.

Results. The results of UV measurements of the dilute peptide solutions (in the range appropriate for CD measurements) are displayed graphically, plotted against the number of solubilizing lysines, in Figure 22a and against concentration as determined on the basis of NMR in Figure 22b. The corresponding numerical data are listed in Table 1. Since no obvious trend for these data is apparent and the data are virtually indistinguishable, they were treated as one large set of 28 points. The average value of ϵ_{280} across the peptide solutions is 5.557×10^3 M^{-1} cm^{-1}. This value agrees well with the experimentally determined ϵ_{280} of free tryptophan amide hydrochloride and acid in both pure water and aqueous NaCl.[57] Indeed, the calculated value of ϵ_{280} is not significantly affected if all data taken in pure water and aqueous NaCl are included (5.553×10^3 M^{-1} cm^{-1}) All values of ϵ_{280} determined in 6 M GuHCl are significantly larger than those determined in the other two contexts, as seen in Table 2.

Error Analysis. As with any measurements involving quantification, there are elements of random error associated with this dataset. An estimate of this error follows. Dry masses weighed on an analytical balance are assigned a maximal error of ±0.0002 g (at most 0.2%). Error associated with the calibrated micropipettor was found to be 0.4%; including random errors, the total partial error of 1% is assigned for the measurement of small volumes by micropipet. Errors associated with volumetric flasks are assumed to be negligible for these purposes. Integration by NMR showed no more than a 2% variation and is therefore assigned an error of 2%. Variations on the Cary UV spectrometer were very small over repeated measurements, including blank scans, but variations in the values of blank scans for particular cells were in the range of 1−2%. Even though blank scans were taken immediately prior to use,

(57) See Supporting Information for any data not shown here.

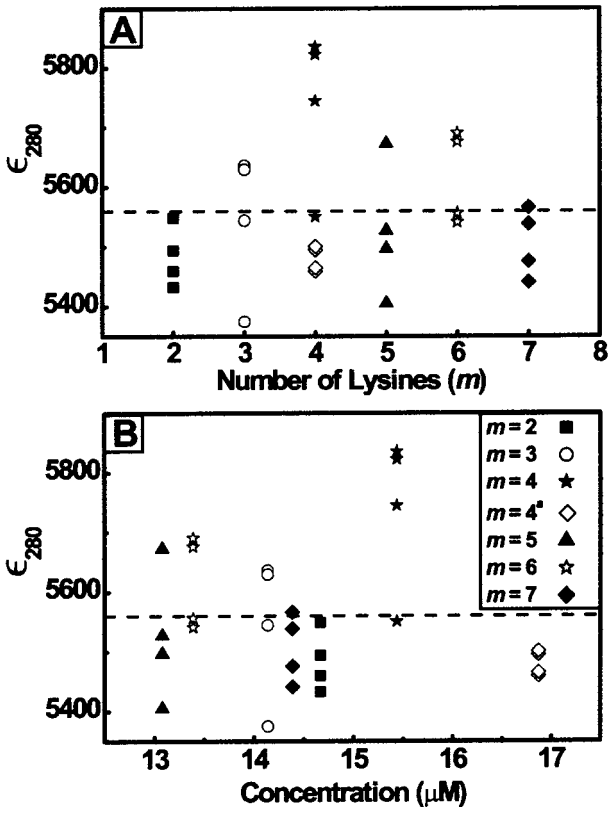

Figure 22. Empirically determined tryptophan ϵ_{280} for $WK_mInp_2{}^tLA_n{}^tLInp_2K_m$ plotted vs solubilizer length *m* (A) and concentration (B). Systematic deviation from the average value of ϵ_{280} (dashed line) is not evident in either plot, and the data are therefore treated as one dataset. The hollow diamonds indicate data acquired for $WK_4Inp_2{}^tL$.

Table 1. Empirical Concentrations and ϵ_{280} for $WK_mInp_2{}^tLA_4{}^tLInp_2K_m$

m	concn (μM)[a]	$\epsilon_{280} \times 10^{-3}$ (M^{-1} cm^{-1})
2	14.67	5.494, 5.549, 5.433, 5.460
3	14.14	5.636, 5.629, 5.545, 5.375
4	15.44	5.551, 5.745, 5.835, 5.823
4[b]	16.87	5.459, 5.495, 5.501, 5.465
5	13.08	5.405, 5.673, 5.497, 5.528
6	14.10	5.541, 5.691, 5.556, 5.676
7	14.39	5.566, 5.476, 5.539, 5.441

[a] Concentrations are based on 1% dilutions of stock solutions as determined by NMR with a *p*-nitrophenol internal standard. [b] For $WK_4Inp_2{}^tL$.

Table 2. Average ϵ_{280} in Various Contexts

	$\epsilon_{280} \times 10^{-3}$ (M^{-1} cm^{-1})		
context	pure water	100 mM NaCl	6 M GuHCl
peptide	5.557	5.627[a]	5.905[a]
amide	5.554	5.545	5.829
acid	5.432	5.497	5.841

[a] Values only for a single peptide ($m = 4$, from Table 1); the associated errors are therefore larger than for the average value indicated in the first column.

a generous random error of 2% is therefore assigned for UV measurements.

Concentrations determined by NMR were calculated as in eq A1:

$$\frac{M_{\text{std}}V_{\text{std}}}{\text{INT}_{\text{std}}} = \frac{M_xV_x}{\text{INT}_x} \qquad \text{(A1)}$$

using the abbreviations std, standard *p*-nitrophenol solution; *x*, stock solution in question; M, molarity; *V*, measured volume of solution; and INT, relative integration of a peak worth a single proton by NMR. Using the rearranged eq A2,

$$M_x = \frac{M_{\text{std}}V_{\text{std}}\,\text{INT}_x}{V_x\,\text{INT}_{\text{std}}} \qquad \text{(A2)}$$

the upper bound of the error associated with M_x is 6.2% using the simple additive errors shown in eq A3:

$$\delta(M_x) = (0.2\% + 1\% + 2\%) + (1\% + 2\%) = 6.2\% \qquad \text{(A3)}$$

Stock solutions were diluted volumetrically, adding an error of 1% for the small volume measurement, giving dilute solutions of concentration M_y. With ϵ_{280} calculated by eq A4,

$$\epsilon_{280} = \frac{\text{ABS}}{M_y} \qquad \text{(A4)}$$

where ABS is the absorbance at 280 nm, the total error has an upper bound of 9.2%, as can be seen in eq A5.

$$\delta(\epsilon_{280}) = 2\% + (6.2\% + 1\%) = 9.2\% \qquad \text{(A5)}$$

A more realistic estimation of error adds all of the partial error terms in quadrature but assumes that errors associated with NMR integrations are not necessarily independent and are therefore additive. The resulting calculated error for each measurement of ϵ_{280} shown in eq A6,

$$\delta(_{280}) = [0.002^2 + 3(0.01^2) + 0.04^2 + 0.02^2]^{1/2} = 4.8\% \qquad \text{(A6)}$$

assuming one balance error, three pipettor errors, two NMR integration errors, and a single UV measurement error is ±4.8% for peptide solutions with concentrations measured by NMR. The error associated with ϵ_{280} measured on solutions containing only recrystallized material is estimated to be considerably smaller because the stock solutions required no small volume measurements, and because NMR integration—by far the largest term—was not used to determine concentrations.

As seen in Table 2, the high (5.835×10^3) and low (5.375×10^3) extrema of ϵ_{280} calculated on the basis of the peptide solutions fall well within the larger bounded error limits, and in fact lie within 5% of the calculated mean, essentially within the small bounded error limits. Inspection of Figure 22 demonstrates, as expected, that most of the data are clustered much closer to the calculated mean than to the extrema. Based on a standard deviation of 0.118×10^3 for the 28-point data set, the value of ϵ_{280} for tryptophan in the context of the solubilized, spaced peptides at 95% confidence is $(5.557 \pm 0.045) \times 10^3$ M^{-1} cm^{-1}.

Discussion. The value of ϵ_{280} obtained for the primary standard H-Trp-NH_2·HCl at CD concentrations is nearly identical to that found in the literature[15] of 5.56×10^3 M^{-1} cm^{-1}, thus validating the methods and instrumentation used in this study. Among simple tryptophan derivatives, the chemical structure and ionization state of the amide hydrochloride are expected to mimic best the peptide context used here. While the data indicate that the ionization state of the free acid (which exists primarily as a zwitterion consisting of an ammonium ion

and a carboxylate) may affect its ϵ_{280}, the effect is small and may also be attributed to data deviations that lie within error limits. Indeed, taken as a set, the data obtained in water and 100 mM NaCl[58] using the peptides, the amide hydrochloride, and the free acid[59] are indistinguishable. The same is not true for the data involving GuHCl. It is clear, based on the data, that ϵ_{280} for tryptophan in 6 M GuHCl is significantly higher than it is in either pure water or low-concentration salt solution. As the presence of such a high concentration of GuHCl probably overrides other local peptide charge contexts, the data from this study measuring the absorbance of the W chromophore in 6 M GuHCl can reasonably be used to assign ϵ_{280} in such a context. Using the methods described above, a value for ϵ_{280} in 6 M GuHCl at 95% confidence is $(5.888 \pm 0.067) \times 10^3\ M^{-1}\ cm^{-1}$.

(58) Although the data obtained in NaCl solution (see Table 2 and Supporting Information) fall outside of the stated 95% confidence limits for ϵ_{280}, they fall well within the expected error for individual points centered around the mean calculated for ϵ_{280} using the peptides, the amide hydrochloride, or both. The data measured in 100 mM NaCl are nevertheless not included in the calculation of ϵ_{280} due to uncertainty regarding the relevance of its context.

(59) See note 58. The same arguments can be made about data using the tryptophan free acid. Data obtained using the free acid are used when calculating ϵ_{280} in 6 M GuHCl.

Conclusions. The UV chromophore of tryptophan can be used reproducibly to determine peptide concentrations of CD-ready solutions. The molar extinction coefficient of tryptophan at 280 nm is invariant in the peptide and buffer contexts employed in this study (up to 100 mM NaCl) but changes under extreme buffer conditions. To use the tryptophan chromophore for concentration determination in different buffer systems, ϵ_{280} must first be measured under those conditions. Additionally, although peptide context in this case does not affect ϵ_{280}, such contexts have not generally been eliminated as potential sources of error in concentration determination. Having eliminated such error here, ϵ_{280} for tryptophan was found in this context to be $(5.557 \pm 0.045) \times 10^3\ M^{-1}\ cm^{-1}$.

Supporting Information Available: Mass spectroscopy data, ellipticity data for peptides with Gly IS regions, analytical ultracentrifugation experimental conditions, tryptophan extinction coefficient data, and information on Lifson−Roig mathematical modeling and calculations using the cooperativity modifications (PDF). This material is available free of charge via the Internet at http://pubs.acs.org.

JA011726D